A novel spatio-temporal method for determining necking and fracture strains of sheet metals

Ruiqiang Zhang [a], Zhusheng Shi [a], Zhutao Shao [a], Trevor A. Dean [b] and Jianguo Lin [a,*]
[a] *Department of Mechanical Engineering, Imperial College London, London SW7 2AZ, UK*
[b] *Department of Mechanical Engineering, University of Birmingham, Birmingham B15 2TT, UK*
* Corresponding author. *Email address:* jianguo.lin@imperial.ac.uk (J. Lin).

Abstract

Forming limit diagrams (FLDs) and fracture forming limit diagrams (FFLDs) have been widely used to evaluate formability of sheet metals. There are many existing methods for determining localised necking strain and fracture strain necessary to construct these diagrams, however, none has been widely accepted and applied to the range of available formability testing methods, e.g. Nakajima tests and biaxial tensile tests. In this study, a novel spatio-temporal method is proposed and developed for determining the localised necking strain and the fracture strain in deformed sheet metals. In the method, localised necking is assumed to appear at the beginning of an increasing difference between average thickness strain within two rectangular zones where localised necking occurs. The effects of dimensions of the two zones on determined localised necking strains were investigated using uniaxial tensile tests for three sheet metals: AA7075, boron steel and AA6082, and the optimal dimensions are recommended to ensure accurate determinations. In comparison with several widely used existing methods, it was concluded that the novel method has greater simplicity, stability and accuracy in determining the localised necking strains. The method was also successfully applied to determine the localised necking strain and the fracture strain for AA5754 in biaxial tensile tests and it was demonstrated to be unaffected by noise and the Portevin–Le Châtelier (PLC) effect.

Keywords: Localised necking; Fracture; Biaxial tensile test; Formability; Forming limit diagram (FLD)

1. Introduction

The demand for complex-shaped components formed from sheet metal has been increasing in recent years, largely in response to a growing need for lightweight structures. In order to optimise work-piece utilization, development of novel forming processes employing as yet unused conditions, has raised the necessity for determining sheet metal characteristics and in particular formability, over a wide range of conditions. The forming limit diagram (FLD), which was firstly proposed by Keeler [1] and Goodwin [2], is the most commonly used tool to represent the formability of sheet materials. An FLD shows, in the space of major and minor strain, the limit strain at onset of localised necking (localised necking strain) [3]. It is obtained by deforming sheets in various proportional strain paths (e.g. uniaxial tension and equi-biaxial tension) under the plane stress condition. The fracture forming limit diagram (FFLD) is an alternative index of formability, obtained by extending an FLD to the limit strain at fracture (fracture strain). It is useful in some circumstances, e.g. in deep drawing of a square cup [4] or in single point incremental forming processing [5], where fracture is likely to limit the attainable deformation. Two major aspects exist in determining either an FLD or FFLD. One is deformation to fracture of work-pieces through various fixed proportional strain paths, using methods such as the Nakajima test [6] and the Marciniak and Kuczynski test [7]; The other is using a method which enables localised necking strain and/or fracture strain to be determined precisely.

Significant efforts have been dedicated for the development of the experimental methods to determine the localised necking strains and a comprehensive summary of them can be found in [8]. They can be classified into three main categories: (1) spatial methods, (2) temporal methods and (3) spatio-temporal methods.

The spatial methods consider only strain distribution after the appearance of failure. The cross-section (CS) method in the ISO standard 12004-2 [9, 10], which originated from [11], is the most widely used spatial method. In this, strain points in the necked area are removed and reconstructed by a best fit with an inverse parabola ($f(x) = 1/(ax^2 + bx + c)$), to the remaining part of strain distribution on both sides of the neck over the defined fit windows. This method has been applied to determine FLDs for sheet metals, together with Nakajima tests [12, 13], for both room temperature and high temperature tests [14, 15]. Another spatial method using digital image correlation (DIC) technique, named DIC-Grid, has been proposed by Zhang et al. [16] and by calculating the deformation of an assumed virtual grid, applied to determining FLDs for QP980 steel [16] and Al-Mg-Si alloy [17].

In temporal methods (or time-dependent methods), either the first or the second time derivative of strains within a local area where necking is leading to fracture is analysed, based on different algorithms. The linear best fit (LBF), which is one of the existing temporal methods, is based on a technology proposed by Volk and Hora [18] and involves analysis of first derivative of thickness strain to identify the onset of localised necking. Huang et al. [19] developed a temporal approach by analysing the major strain acceleration (so named 'second derivative approach') within a localised necking zone, and adopting the abrupt change in the major strain rate, to represent strain localisation within the neck, which is identified by a peak in the curve of major strain acceleration versus time. The temporal method, correlation coefficient (CC), proposed by Merklein et al. [20] utilises the same concept that the major strain within a localised neck accelerates upon localised necking, and a correlation coefficient, which expresses the quality of a linear approximation, is adopted to identify the increase of the strain rate automatically. The gliding correlation coefficient (GCC) method [21] is an improved CC method which overcomes the mathematical instability in calculating the correlation coefficient by adding a linear function to the major strain acceleration. The gliding difference of mean to median (GDMM) method [21] utilises the difference between a gliding mean and a gliding median over a number of frames to identify a sharp change in thickness strain rate, which is assumed to be the beginning of unstable necking.

The spatio-temporal methods are combinations of spatial methods and temporal methods, which take into account the time-dependent strain fields. The critical ratio (CR) method, which is based on a technology proposed by Marciniak and Kuczynski [7], is a typical spatio-temporal method. In this, localised necking is assumed to occur when thickness strain increment ratio between a local area located in the localised necking zone and a local area in an adjacent zone attains a critical value. This generally varies from 7 [22] to 10 [23] in the literature. Applications of the CR method can be found for determination of FLDs for alloys, aluminium alloy 5086 (AA5086) [24-26] and DP600 [27]. Wang et al. [17] proposed a spatio-temporal method based on the concept that localised necking generates non-uniform deformation through the specimen thickness [3], and the onset of localised necking is identified as the start of a sharp increase in surface height difference between a point in a localised neck and a point away from the necking area. Min et al. [8] also proposed a spatio-temporal method, referred to as a 2D curvature method, using which onset of localised necking can be identified by evaluating surface curvature, fitted from surface coordinate data extracted over a narrow surface. They later applied the method to test-pieces deformed in Nakajima tests [10]. Based on the physical

phenomenon of localised necking, that an unstable local reduction appears in the sheet thickness, Martínez-Donaire et al. [28] developed a novel method to identify the onset of localised necking by analysing the evolution of the major strain rate for a series of aligned points along a section perpendicular to the crack. Iquilio et al. [29] utilised the same methodology, but analysed the thickness strain rate under the assumption of incompressibility.

Despite the abundance of the existing methods to determine localised necking strains, no method has been universally accepted so far. Comparisons of several popular existing methods with respect to stability and accuracy can be found in [21, 30]. Indeed, the CS method has been used for several decades because of validity. However, extreme conditions for curve fitting in the CS method easily lead to incorrect mathematical evaluations. For example, the CS method is inapplicable for some materials, such as high strength steels and some aluminium alloys, due to non-homogeneous deformation even before the occurrence of localised necking [21]. The CS method also requires that the width of the fit window should be at least 4 mm on each side of the crack, which makes the method inapplicable in biaxial tensile tests in which effective gauge region is generally smaller [26, 27]. It seems that time-dependent methods have a wider range of application. However, calculation of either first derivative or second derivative of strain may be strongly influenced by noise or other factors, such as the PLC effect in austenitic steel [31] and aluminium alloy AA5000 series [32, 33].

With respect to methods for determining fracture strains, no standard has been set and no method has been widely accepted. Gorji et al. [34] introduced a thinning method to measure fracture strain under assumption of plane strain state, which is based on the microscopic measurements of rupture regions. The measured fracture strain using the thinning method is higher than that using the DIC method. Panich et al. [35] determined the FFLD for DP980 steel sheet, using Nakajima tests, in which the principal strains within a localised neck at the final stage, immediately before fracture, were taken as the fracture strains. This method was also applied by Park et al. [36] to determine the FFLD for DP980 steel sheet in hydraulic bulge tests. Luo et al. [37] determined fracture strains by utilising the reverse engineering method, which had been used by Bao and Wierzbicki [38] and Wierzbicki et al. [39] for the same purpose. However, determined values of fracture strain probably are influenced by the adopted constitutive models. Other methods can also be found, in which fracture strains were determined by measuring adhesive grids placed just outside the crack [40] or measuring thickness and width in the fracture region of deformed specimens [41, 42].

The aim of this study is to develop a novel reliable spatio-temporal method to determine the localised necking strain and the fracture strain for constructing an FLD and FFLD for sheet metals deformed in various formability tests, e.g. biaxial tensile tests. The validity of the spatio-temporal method was investigated and evaluated by determining localised necking strains in uniaxial tensile tests for three sheet metals: AA7075, boron steel and AA6082. Both the simplicity and the stability of the method were evaluated and discussed by comparing it with several widely used existing methods. The spatio-temporal method was applied also to determine the localised necking strain and the fracture strain of AA5754 sheet, deformed using a biaxial tensile test.

2. The novel spatio-temporal method

In sheet metal forming, localised necking usually appears after onset of diffuse necking and terminates at fracture [43]. According to the Hill's criterion [44], a necking band forms along the zero extension direction. That is, after the onset of localised necking, deformation mainly continues in normal direction of the necking band [45]. Based on the physical mechanism of localised necking, a

novel spatio-temporal method is proposed to identify the onset of localised necking and then to determine the localised necking strain, which is schematically illustrated in Fig. 1. Assuming that strain fields in a deformation have been measured using DIC technique, as shown in Fig. 1(a), two rectangular zones, named base zone (BZ) and reference zone (RZ), are selected on the last image immediately before fracture, in which a necking band appears, and are then transferred to the first image at the start of the deformation. Zones BZ and RZ have a same central point at which localised necking initiates, a same dimension W_{L} in the parallel direction to necking band, and different dimensions W_{BZ} and W_{RZ} ($W_{\mathrm{RZ}} > W_{\mathrm{BZ}}$) respectively, in the normal direction to necking band. Therefore, there must be an increasing difference between absolute values of average thickness strain within the two zones ($\left|\varepsilon_3^{\mathrm{BZ}}\right|$ and $\left|\varepsilon_3^{\mathrm{RZ}}\right|$) once necking happens. In the spatio-temporal method, localised necking is assumed to appear when the increasing difference starts. Fig. 1(b) presents the way to identify the beginning of the increasing difference in the space of $\left|\varepsilon_3^{\mathrm{BZ}}\right|$ and $\left|\varepsilon_3^{\mathrm{RZ}}\right|$. Two straight lines are fitted: one through the points before necking appears, of which the slope *k* is in value of one because $\left|\varepsilon_3^{\mathrm{BZ}}\right|$ and $\left|\varepsilon_3^{\mathrm{RZ}}\right|$ are equal, and the other through the last three points immediately before fracture. The reason for selecting the last three points is that those points are easy to be determined and as shown later, most other points after the determined necking time are on the fitted line. Intersection of the two fitted lines is treated as the beginning of the increasing difference and as the onset of localised necking. This is based on the mechanism that before necking, $\left|\varepsilon_3^{\mathrm{BZ}}\right|$ is equal to $\left|\varepsilon_3^{\mathrm{RZ}}\right|$ because of uniform deformation, while the occurrence of necking results in that $\left|\varepsilon_3^{\mathrm{BZ}}\right|$ becomes higher and higher than $\left|\varepsilon_3^{\mathrm{RZ}}\right|$. Similar approach has been used in the method of Linear Best Fit [18,21]. Consequently, the strains within zone BZ at the corresponding time are determined as the localised necking strain. In the current study, the zone RZ includes zone BZ due to more stable and reasonable results, as demonstrated in Appendix A1. The spatio-temporal method also enables the determination of the fracture strain from zone BZ at the time immediately before fracture. The method considers both the temporal evolution of strain, and the strain distribution perpendicular to the fracture direction. This differs from temporal methods which only consider the temporal evolution of strain, as mentioned by Min et al. [8]. Thus, the proposed method is a spatio-temporal method.

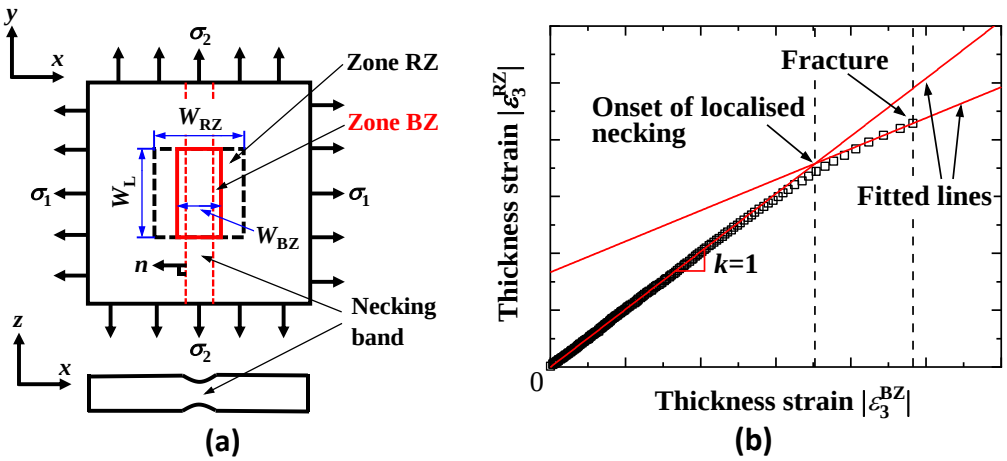

Fig. 1. Schematic diagrams illustrating the novel spatio-temporal method for determination of onset of localised necking: (a) selection of zones BZ and RZ on deformed test pieces where a necking band appears, in which the zones BZ and RZ have a same dimension W_{L} in parallel direction to necking band, and have different dimensions W_{BZ} and W_{RZ} ($W_{\mathrm{RZ}} > W_{\mathrm{BZ}}$) in normal direction to necking band, and (b) determination of onset of localised necking by identifying the beginning of an increasing difference between absolute values of thickness strain $\left|\varepsilon_3^{\mathrm{BZ}}\right|$ and $\left|\varepsilon_3^{\mathrm{RZ}}\right|$ within the two zones.

In summary, the following procedure is performed to determine the localised necking strain and the fracture strain of deformed sheet metals using the novel spatio-temporal method:

i. Measure strain fields using the DIC technique;
ii. Select rectangular zones BZ and RZ in the last image immediately before fracture, in which a necking band can be observed, and then transferring them to the first image when the deformation starts. The two zones have a same central point where localised necking initiates, a same dimension W_{L} in the parallel direction to necking band, and different dimensions W_{BZ} and W_{RZ} ($W_{\mathrm{RZ}} > W_{\mathrm{BZ}}$) in the normal direction to necking band, as shown in Fig. 1(a);
iii. Determine the onset of localised necking by identifying the beginning of an increasing difference between $\left|\varepsilon_3^{\mathrm{BZ}}\right|$ and $\left|\varepsilon_3^{\mathrm{RZ}}\right|$, as shown in Fig. 1(b);
iv. Determine the time at the onset of localised necking and the time immediately before fracture;
v. Determine the localised necking strain and the fracture strain from zone BZ at the corresponding times, separately.

3. Experimental details

3.1. Uniaxial tensile tests

Uniaxial tensile tests were conducted for three sheet metals: 1.8 mm thick AA7075, 1.5 mm thick boron steel 22MnB5 and 1.5 mm thick AA6082. Dog-bone shaped specimens were cut along the rolling direction of the as-received sheet and were ground and polished to minimise stress concentration at specimen edge, so that edge cracking in gauge length can be avoided until localised necking occurs during testing, which has been carefully monitored for all tested samples. To check the independence of the application of the spatio-temporal method on specimen geometry and dimension, two different specimen designs were utilised. They are shown in Fig. 2(a) for AA7075 and boron steel, and in Fig. 2(b) for AA6082. A Gleeble thermal-mechanical simulator (3800) was used to perform the tests at a constant speed of 15 mm/min, and the DIC technique was adopted to measure the strain fields in the reduced parallel section of each specimen at a constant frame rate of 125 frames per second (fps).

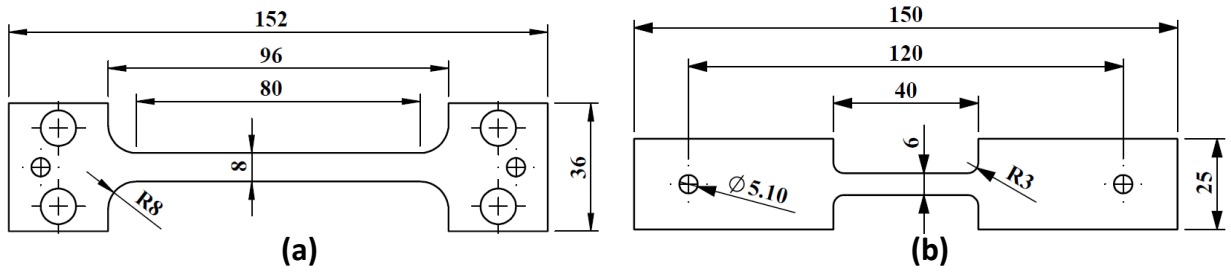

Fig. 2. Geometry and dimensions of dog-bone shaped specimens for (a) AA7075 and boron steel, and (b) AA6082.

3.2. Biaxial tensile tests

Biaxial tensile tests were carried out for 1.5 mm thick AA5754 using a novel biaxial testing system [46], in which a patented planar biaxial tensile rig [47], as shown in Fig. 3(a), is capable of converting an input uniaxial force into output biaxial forces, thereby stretching cruciform specimens. Figs. 3(b1)-(b2) illustrate plane-strain tension and equi-biaxial tension respectively, achieved within the

capability of the patented rig, for deformations under different strain states. Details of the mechanism of the patented rig are given in [46]. Fig. 3(c) shows the geometry and dimensions of the cruciform specimens, in which the thickness in the central region was reduced in order to concentrate deformation and ensure fracture occurred in the gauge region. All cruciform specimens were deformed by keeping the relative speed of two opposing grips constant as 15 mm/min. The DIC technique was used to measure the strain fields in the central region of each cruciform specimen, at a constant frame rate of 125 fps.

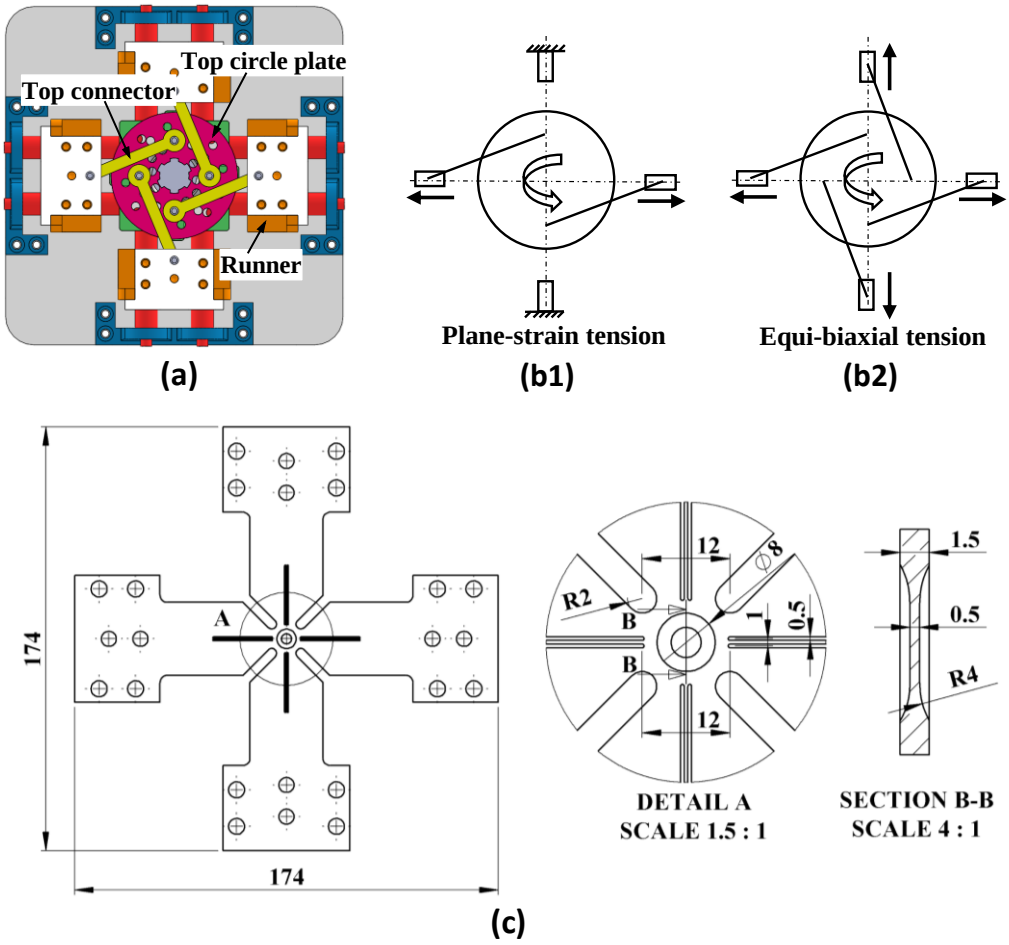

Fig. 3. A planar biaxial tensile rig and cruciform specimen design for biaxial tensile tests: (a) front view of the patented planar biaxial tensile rig for cruciform specimen deformations [46, 47], (b1)-(b2) schematic illustrations of rig connector set-up to realise (b1) plane-strain tension and (b2) equi-biaxial tension, and (c) geometry and dimensions of a cruciform specimen.

4. Determination of limit strains using the spatio-temporal method

4.1. Effects of W_{BZ} and W_{RZ} on determined localised necking strains

In order to determine the optimal dimensions W_{BZ} and W_{RZ}, their effects on determined localised necking strains were investigated by adopting various sizes of zones BZ and RZ to determine localised necking strains in uniaxial tensile tests for the three sheet alloys: AA7075, boron steel and AA6082.

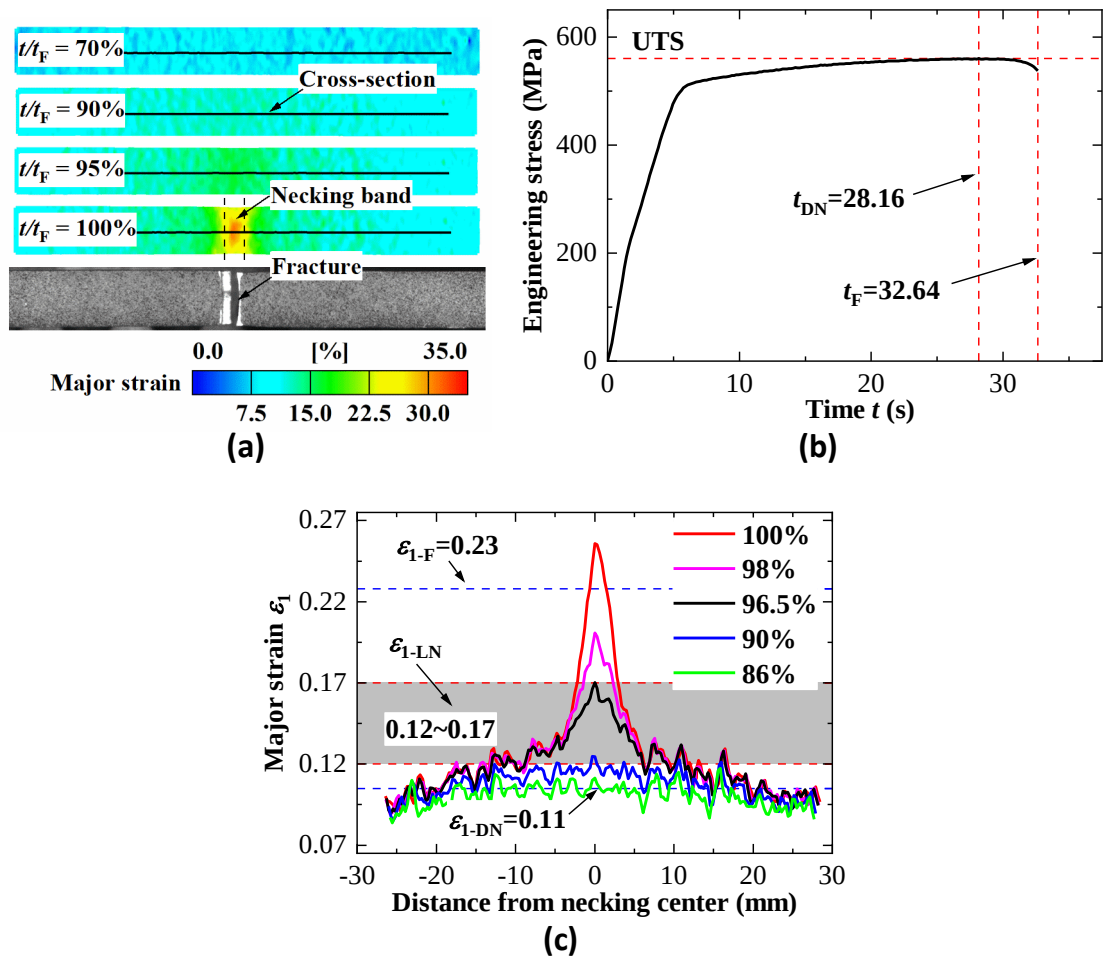

Fig. 4. Necking development and strain evolution in uniaxial tensile test for AA7075 sheets: (a) major strain contours in the reduced parallel section of a dog-bone specimen at normalised times t/t_F of 70%, 90%, 95% and 100%, (b) measured engineering stress vs. time curve for AA7075, and (c) major strain distribution along a cross-section in the specimen, as indicated in (a), at different normalised times.

Case A: AA7075

Fig. 4(a) shows the major strain (engineering) contours in a dog-bone specimen of 1.8 mm thick AA7075, deformed during a uniaxial tensile test, in which 70%, 90%, 95% and 100% are normalised times t/t_F, where t is current time and t_F is fracture time. In the strain contour at t/t_F = 100%, a well-developed necking band, where a maximum deformation occurred, was observed in the reduced parallel section of the specimen. According to the flat fracture shape (90° to the tensile direction), the failure of the material is probably controlled by the maximum principal stress. Similar phenomenon has been reported previously [48]. It should be noted that the time gap between the last image right before fracture (t/t_F = 100%) and the fracture image is only 8 ms in the current study, i.e., the strain contour at t/t_F = 100% is able to show what the material exhibits. The diffuse necking time (t_{DN}) was determined according to the Considère criterion [49] that in uniaxial loading, diffuse necking begins when stress reaches the ultimate tensile strength (UTS). Fig. 4(b) presents the curve of engineering stress versus time for AA7075 in the uniaxial tensile test, with the diffuse necking time t_{DN} = 28.16 s which corresponds to a normalised time of 86%. Fig. 4(c) shows the major strain distribution along the cross-section (as indicated in Fig. 4(a)) after the onset of diffuse necking, at t/t_F = 86%, 90%, 96.5%, 98% and 100%. It can be seen that necking proceeds from being diffuse and gradually concentrates to a single band before fracture, and strain distribution at t/t_F = 100 % shows that the necking band is highly localised. In uniaxial tensile tests, strains are homogeneous

before onset of diffuse necking, so the major strain at the onset of diffuse necking ($\varepsilon_{1-\mathrm{DN}}$) is independent of gauge length [43]. However, the major strain at fracture ($\varepsilon_{1-\mathrm{F}}$) is highly sensitive to gauge length due to heterogeneous strain distribution around the necking band at the fracture time t_{F}. In this study, $\varepsilon_{1-\mathrm{F}}$ was calculated in a gauge length of $2 \times h$ as a reference, where h is the thickness of the material. For AA7075, $\varepsilon_{1-\mathrm{DN}}$ and $\varepsilon_{1-\mathrm{F}}$ determined in such a way are 0.11 and 0.23 respectively. In uniaxial tensile tests for flat samples, it is well known that diffuse necking starts when the tensile load reaches its maximum, followed by localised necking until fracture [50]. After the onset of the localised necking, the deformation begins to concentrate in a narrow band of width that is often of the order of test-piece thickness [44, 51]. Therefore, the range of onset of localised necking must be higher than diffuse necking time but smaller than fracture time, and can be estimated roughly as a reference [45]. According to necking development mechanism and the strain distribution shown in Fig. 4(c), it was estimated that localised necking began at a normalised time between 90% and 96.5%. Therefore, the major strain at the onset of localised necking ($\varepsilon_{1-\mathrm{LN}}$) would be in the range of 0.12 to 0.17, as seen in Fig. 4(c).

Various zone BZ and RZ values were selected to evaluate the effects of their dimensions orthogonal to necking band on the determined localised necking strains, as presented in Table 1. To carry out sensitive studies and to determine necking strain close to the estimated necking strain range, values of W_{BZ} were chosen as $1.5 \times h$, $2 \times h$, $2.5 \times h$ and $3 \times h$, namely 2.7, 3.6, 4.5 and 5.4 mm respectively, and the corresponding W_{RZ} was chosen to make the ratio $R = W_{\mathrm{RZ}}/W_{\mathrm{BZ}}$ = 1.5, 2, 2.5 and 3. As shown in Appendix A2, W_{L} values from $1.5 \times h$ to $3 \times h$ have little effect on the strain results. Based on the sensitivity studies, the same value $W_{\mathrm{L}} = 2 \times h$ was used for all zones BZ and RZ in this study.

Table 1. Selected dimensions of zones BZ and RZ.

W_{BZ}	$R = W_{\mathrm{RZ}}/W_{\mathrm{BZ}}$	W_{L}
$1.5 \times h$ $2 \times h$ $2.5 \times h$ $3 \times h$	1.5, 2, 2.5 and 3	$2 \times h$

Fig. 5(a) shows identification of onset of localised necking by adopting one zone BZ with W_{BZ} = 3.6 mm and four zones RZ with W_{RZ} = 5.4, 7.2, 9 and 10.8 mm respectively. As expected, the absolute values of average thickness strain within zone BZ ($\left|\varepsilon_3^{\mathrm{BZ}}\right|$) and within any one of the zones RZ ($\left|\varepsilon_3^{\mathrm{RZ}}\right|$), increased at the same rate initially. After a time, however, the increasing rate of $\left|\varepsilon_3^{\mathrm{BZ}}\right|$ gradually became higher than that of $\left|\varepsilon_3^{\mathrm{RZ}}\right|$, and thus an increasing difference between $\left|\varepsilon_3^{\mathrm{BZ}}\right|$ and $\left|\varepsilon_3^{\mathrm{RZ}}\right|$ arose. Furthermore, with increasing W_{RZ} from 5.4 to 10.8 mm, the slope of the fitted lines denoting unstable deformation (the last three points immediately before fracture) decreased. This is because the deformation after the onset of necking is nonuniform, and a smaller $\left|\varepsilon_3^{\mathrm{RZ}}\right|$ was measured within a larger RZ. Consequently, different values of $\left|\varepsilon_3^{\mathrm{BZ}}\right|$ were identified at the start of the divergence of the two strains, caused by different values of zone RZ.

Based on the identified values of $\left|\varepsilon_3^{\mathrm{BZ}}\right|$, the localised necking times (t_{LN}) were determined, as seen in Fig. 5(b). It is noteworthy that $\left|\varepsilon_3^{\mathrm{BZ}}\right|$ increased at a much higher rate after the onset of diffuse necking. This indicates that the way to identify $\left|\varepsilon_3^{\mathrm{BZ}}\right|$ and then determine t_{LN} is beneficial to decrease the scatter among the determined t_{LN}. Fig. 5(c) shows the determined localised necking times t_{LN}. It is

seen that with increasing W_{RZ} (or the ratio R), t_{LN} decreased, while the maximum difference between the times is less than 2%. Based on the determined t_{LN}, localised necking strains (ε_{2-LN}, ε_{1-LN}) were determined by using the strains within zone BZ at the corresponding times, where ε_{2-LN} is the minor strain at onset of localised necking, as presented in Fig. 5(d). It is shown that both $|\varepsilon_{2-LN}|$ ($\varepsilon_{2-LN} < 0$) and ε_{1-LN} decreased with increasing W_{RZ}. Specifically, a highest ε_{1-LN} of 0.162 was determined with W_{RZ} = 5.4 mm, about 15% higher than a lowest ε_{1-LN} of 0.141 obtained with W_{RZ} = 10.8 mm. It is worth noting that the ratio $\varepsilon_{2-LN}/\varepsilon_{1-LN}$ is about -0.32 due to the anisotropy of the material - AA7075, which is different from -0.5 as expected in uniaxial tensile tests.

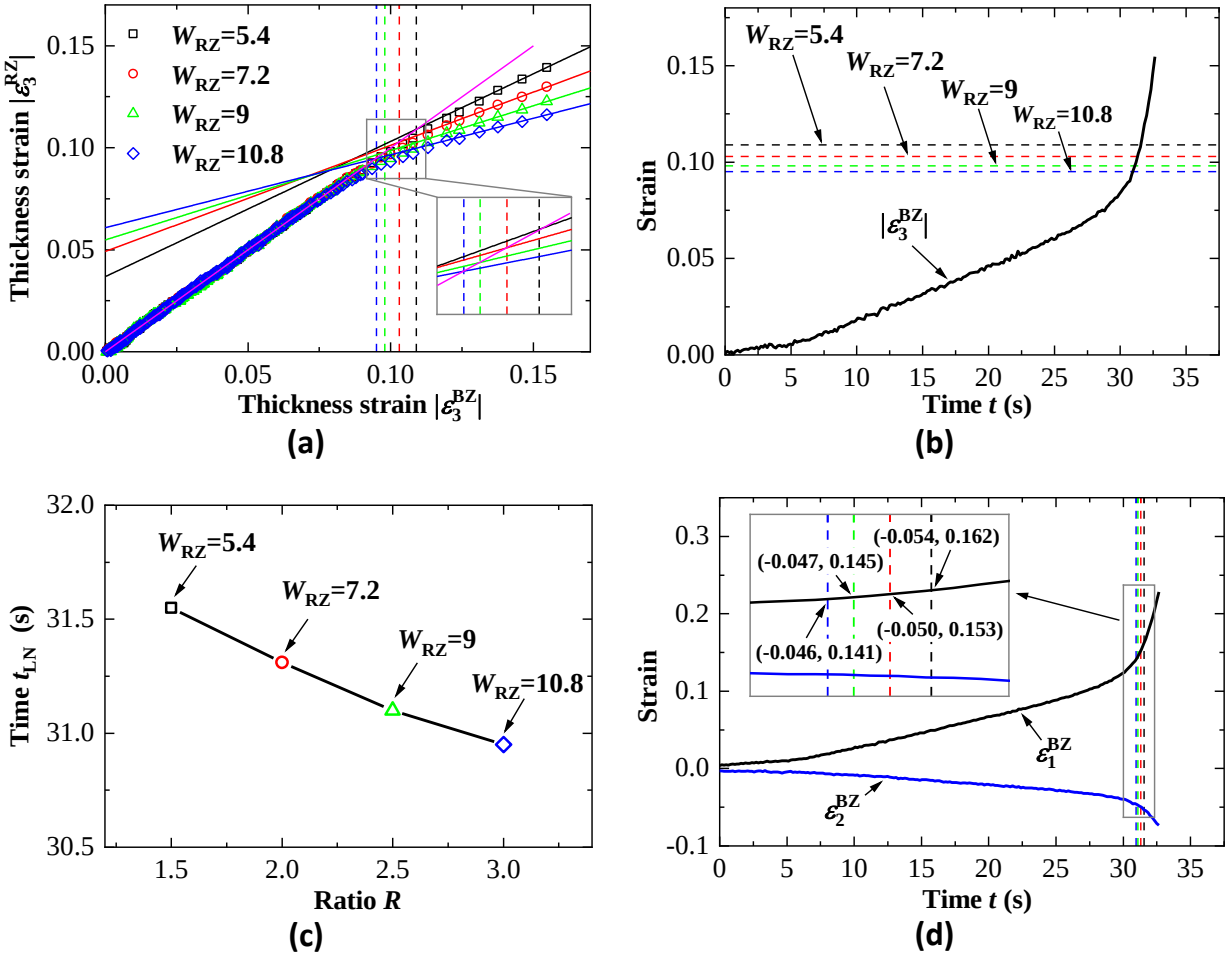

Fig. 5. Effect of dimension W_{RZ} of zone RZ on determined localised necking strains of AA7075 sheets, tested in uniaxial tension, by using the novel spatio-temporal method with a constant W_{BZ} = 3.6 mm and four indicated different W_{RZ} values: (a) identifications of onset of localised necking, (b) identified values of $|\varepsilon_3^{BZ}|$ at the onset of localised necking, (c) determined localised necking times t_{LN} and (d) determined localised necking strains (ε_{2-LN}, ε_{1-LN}), corresponding to the different W_{RZ} values separately.

The other zones BZ and RZ in Table 1 were also adopted to determine, using the spatio-temporal method, the localised necking strain for AA7075. A comparison of the determined localised necking times t_{LN} for various zone BZ and zone RZ values, is plotted in Fig. 6(a). As expected, t_{LN} decreased with increasing W_{BZ} (or ratio R), but the maximum difference among the times is less than 5%. Fig. 6(b) shows the strain paths to fracture for different zone BZ values. Although ε_{1-F} is higher for smaller zone BZ value, the strain paths in different zones BZ are linear and have a same slope. This means that the ratio $\varepsilon_2^{BZ}/\varepsilon_1^{BZ}$ in any point on the strain paths has a same value, and thus it is reasonable to compare only ε_{1-LN} to quantify the difference between localised necking strains determined by

adopting the various zone BZ and RZ values. This is plotted in Fig. 6(c). It is shown that $\varepsilon_{1-\mathrm{LN}}$ decreased with increasing W_{BZ} and ratio R. Specifically, $\varepsilon_{1-\mathrm{LN}}$ decreased from a value 0.174 with W_{BZ} = 2.7 mm and R = 1.5 to a value 0.126 with W_{BZ} = 5.4 mm and R = 3. Moreover, $\varepsilon_{1-\mathrm{LN}}$ is close to the upper and lower bounds of the previously determined range of 0.12 to 0.17 with W_{BZ} = 2.7 and 5.4 mm respectively. This indicates that adopting a small W_{BZ} or a large W_{BZ} may overestimate or underestimate the localised necking strain, respectively.

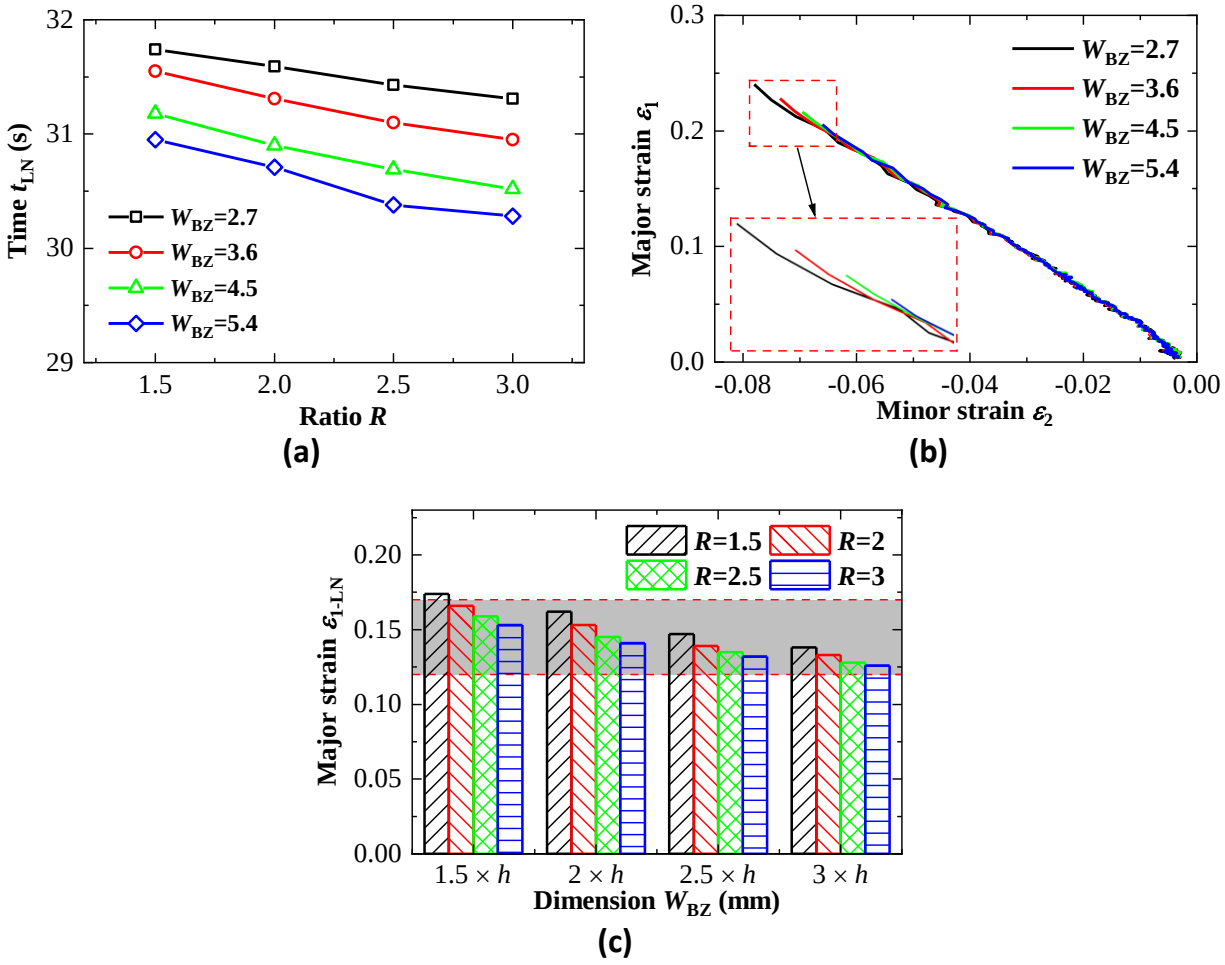

Fig. 6. Effect of dimension W_{BZ} and ratio R ($R = W_{\mathrm{RZ}}/W_{\mathrm{BZ}}$) of zones BZ and RZ on determined localised necking strains of AA7075 sheets tested in uniaxial tension: (a) comparison of determined localised necking time t_{LN} with indicated different W_{BZ} and R values, (b) strain paths to fracture in the zones BZ with the different W_{BZ} values, and (c) effect of W_{BZ} and R on determined major strains $\varepsilon_{1-\mathrm{LN}}$ at onset of localised necking.

Case B: Boron steel

The novel method was also used to determine the localised necking strain for 1.5 mm thick boron steel 22MnB5, uniaxially tensile tested. Edge cracking was not observed in the tested samples before the appearance of necking and fracture occurred randomly within the gauge length. Fig. 7(a) shows the major strain contours in the parallel portion of a dog-bone specimen at normalised times t/t_{F} = 70%, 90%, 95% and 100%. A well-developed necking band is seen at t/t_{F} = 100% with about 45° to the tensile direction and the material fails due to maximum shear stress according to the inclined fracture shape. It has been reported that edge quality of steel specimens affects tensile properties and fracture patterns significantly [52]. The current specimens were carefully ground and polished so that the influence of possible edge cracking is minimised. The curve of engineering stress versus time is plotted in Fig. 7(b) and the diffuse necking time t_{DN} = 37.28 s which corresponds to a normalised

time of 73.5%. Fig. 7(c) shows the major strain distribution along the cross-section (Fig. 7(a)) after the onset of diffuse necking at t/t_F = 73.5%, 89%, 95.5%, 97% and 100%. Using the same method described above for AA7075, ε_{1-DN} and ε_{1-F} were determined as 0.14 and 0.43, respectively. Based on the strain distribution shown in Fig. 7(c), it was judged that localised necking started at a normalised time between 89% and 95.5%. Therefore, a range of 0.20 to 0.28 was determined for ε_{1-LN}. In determining localised necking strain using the spatio-temporal method, various zone BZ values with W_{BZ} = 1.5 × h (2.25 mm), 2 × h (3 mm), 2.5 × h (3.75 mm) and 3 × h (4.5 mm) and various zone RZ values with R = 1.5, 2, 2.5 and 3 were adopted. All zones BZ and RZ have the same dimension W_L = 2 × h (3 mm). Considering the same ratio $\varepsilon_{2-LN}/\varepsilon_{1-LN}$, the difference between determined localised necking strains was quantified by comparing only ε_{1-LN}, as seen in Fig. 7(d). Consistent with the observations in AA7075, ε_{1-LN} was decreased by increasing either the dimension W_{BZ}, or ratio R. Specifically, ε_{1-LN} was decreased from a value of 0.302 with W_{BZ} = 2.25 mm and R = 1.5 to a value of 0.230 by increasing W_{BZ} and R to 4.5 mm and 3 respectively. Moreover, ε_{1-LN} is close to the upper and lower bounds of the range of 0.20 to 0.28 when the dimension W_{BZ} is 2.25 and 4.5 mm respectively.

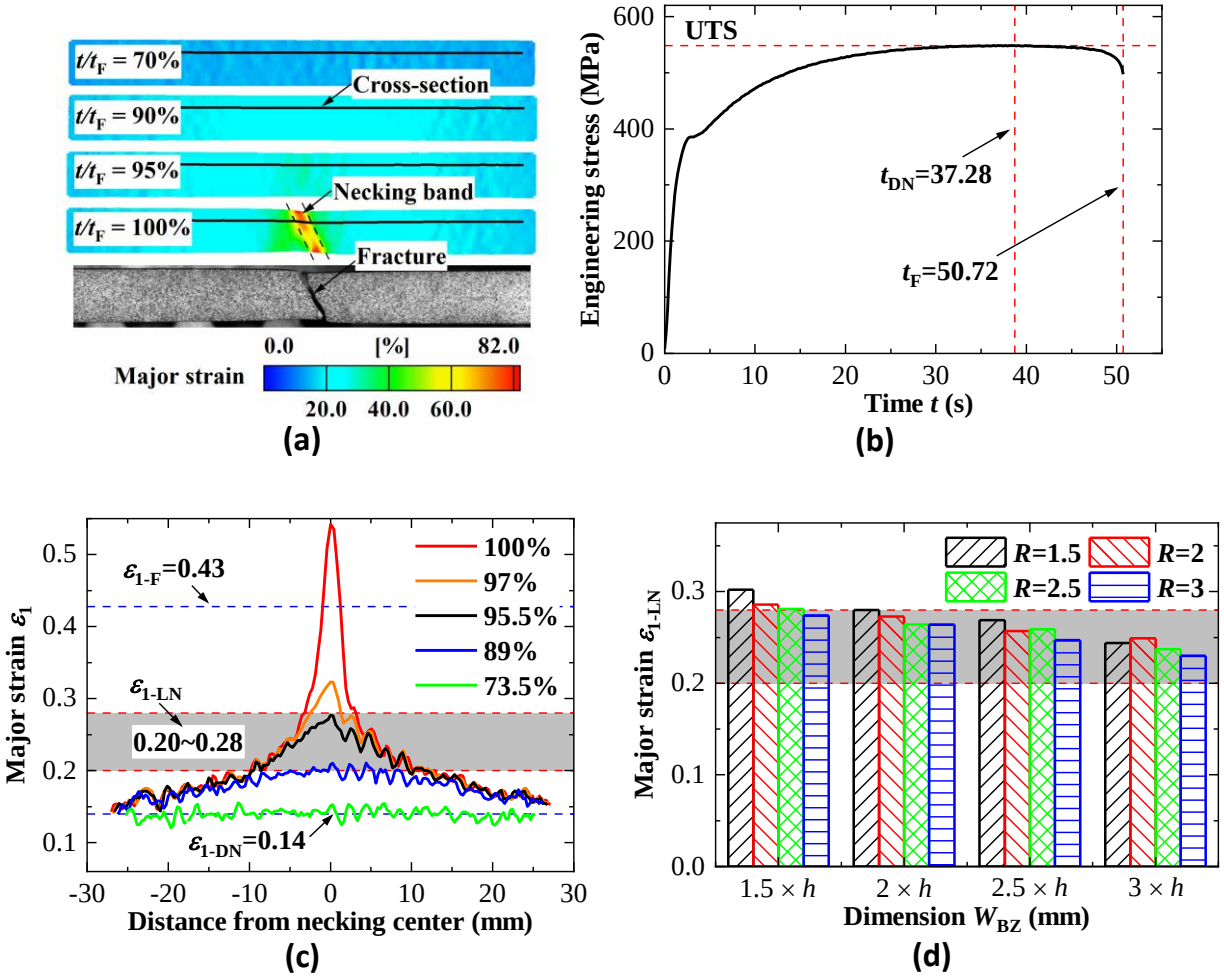

Fig. 7. Effect of dimension W_{BZ} and ratio R ($R = W_{RZ}/W_{BZ}$) of zones BZ and RZ on determined localised necking strains of boron steel 22MnB5 sheets tested in uniaxial tension: (a) major strain contours in the reduced parallel section of a dog-bone specimen at different normalised times, (b) measured engineering stress vs. time curve for boron steel, (c) major strain distribution along a cross-section in the specimen, as indicated in (a), at different normalised times, and (d) effect of W_{BZ} and R on determined major strains ε_{1-LN} at onset of localised necking.

Case C: AA6082

The spatio-temporal method was also used to determine localised necking strain for 1.5 mm thick AA6082 deformed in a uniaxial tensile test. A well-developed necking band was found in the major strain contour (Fig. 8(a)) at t/t_F = 100%, and t_{DN} was determined as 14 s which corresponds to a normalised time of 78% (Fig. 8(b)). Similar to AA7075, the fracture shape is normal to the tensile direction. The major strain distribution along the cross-section (Fig. 8(a)) at t/t_F = 78%, 85%, 92.5%, 95% and 100% is presented in Fig. 8(c), with ε_{1-DN} = 0.12 and ε_{1-F} = 0.29. Based on the strain distribution, it was judged that localised deformation started at a normalised time between 85% and 92.5%. Therefore, a range of 0.14 to 0.20 was determined for ε_{1-LN}. In determining the localised necking strain by using the spatio-temporal method, various zone BZ and RZ values with the same dimensions used for boron steel, were adopted, as test-piece thickness was the same for the two alloys. The difference between determined localised necking strains was quantified by comparing only ε_{1-LN}, as seen in Fig. 8(d). Consistent with the observations for AA7075 and boron steel, a tendency for ε_{1-LN} to decrease with increasing dimension W_{BZ} and the ratio R, is seen. Also, when W_{BZ} = 2.25 and 4.5 mm, ε_{1-LN} is close to the upper and lower bounds of the range of 0.14 to 0.20, respectively. It should be noted that ε_{1-LN} corresponding to W_{BZ} = 2.25 mm and R = 1.5 is at least 25% higher than that for the same W_{BZ} and the other higher R values. This is due to the influence of the noise originated from the DIC measurement on ε_3^{BZ} and ε_3^{RZ} when the dimensions of BZ and RZ zones are too small, as illustrated in Fig. 8(c).

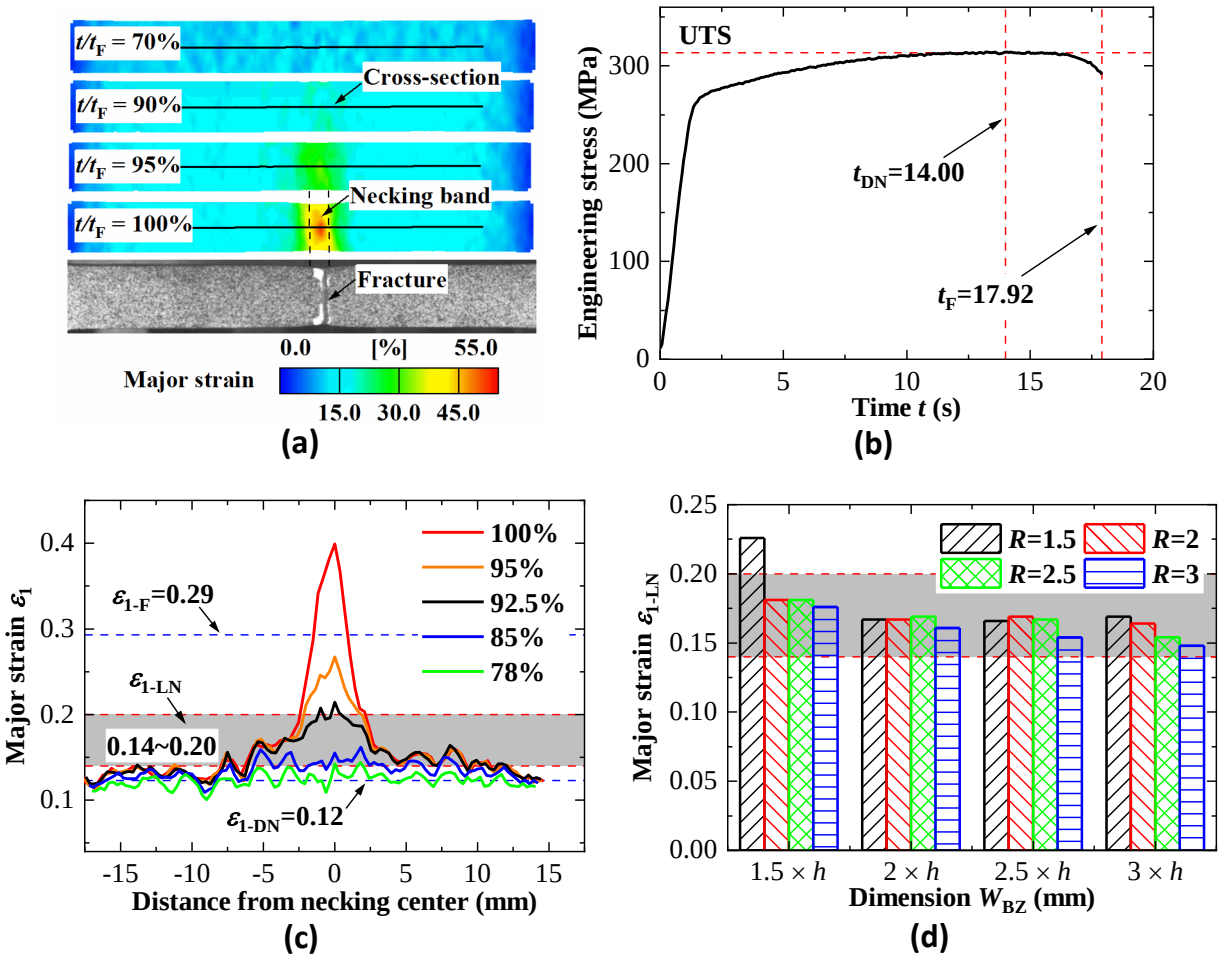

Fig. 8. Effect of dimension W_{BZ} and ratio R ($R = W_{RZ}/W_{BZ}$) of zones BZ and RZ on determined localised necking strains of AA6082 sheets tested in uniaxial tension: (a) major strain contours in the reduced parallel section of a dog-bone

specimen at different normalised times, (b) measured engineering stress vs. time curve for AA6082, (c) major strain distribution along a cross-section in the specimen, as indicated in (a), at different normalised times, and (d) effect of W_{BZ} and R on determined major strains $\varepsilon_{1-\mathrm{LN}}$ at onset of localised necking.

In summary, based on the above investigation of the effects of the dimensions W_{BZ} and W_{RZ} on the determined localised necking strain in the uniaxial tensile tests for the three sheet metals: AA7075, boron steel and AA6082, the optimal dimensions of zones BZ and RZ are recommended, as shown in Table 2. The dimension W_{L} in the recommended range has little effect on the thickness strain within zones BZ and RZ, as shown in Appendix A2. It should be noted that there may be reasonable critical values related to the thickness and plasticity of materials deforming at different conditions, which could be considered in the future recommended standard.

Table 2. Recommended values for the dimensions of zones BZ and RZ.

Dimension	Recommended value
W_{BZ}	$a \cdot h$, a = 2~2.5
W_{RZ}	$b \cdot W_{\mathrm{BZ}}$, b = 2~2.5
W_{L}	$c \cdot h$, c = 1.5~3

4.2. Comparison with existing methods in determining localised necking strains

In this subsection, the novel spatio-temporal method is evaluated against several widely used existing methods by determining localised necking strains in uniaxial tensile tests for the three materials: AA7075, boron steel and AA6082. The existing methods include CS method [9], CR method [7], LBF method [18], CC method [20], GCC method [21], and GDMM method [21].

Fig. 9 presents the applications of the existing methods to the determination of the localised necking strain for AA7075 in uniaxial tensile test, using a script implemented in the commercial software ARAMIS (Company GOM, Germany). As shown in Fig. 9(a), using the CS method, the strain points within the necked area along a predefined cross section were removed and reconstructed by a best fit with an inverse parabola, and then the localised necking strain was determined by the values of the parabola in the crack position. In the application of the CR method, as shown in Fig. 9(b), two zones with dimensions, 3.6 × 3.6 mm were selected on the specimen surface before deformation. One is named inside zone (IZ) where localised necking occurs, and another is named outside zone (OZ) which is 10 mm away from the IZ along the length direction of the specimen. A time interval of 2 s was chosen to calculate the ratio of the thickness strain increment ($r = \mathrm{d}|\varepsilon_3^{\mathrm{IZ}}|/\mathrm{d}|\varepsilon_3^{\mathrm{OZ}}|$) in order to reduce the influence of noise, and a critical ratio value of 7, which has been widely used in the literature, was adopted to identify the onset of localised necking. It should be noted that the influence of noise on the calculation of the ratio cannot be eliminated, as seen in Fig. 9(b).

When using the LBF method, as shown in Fig. 9(c), a local area (red) where the thickness strains increased sharply in respect of the surrounding area, was selected. In order to reduce the influence of noise, a fitting window of 7 points in time was chosen to calculate the thickness strain rate ($\mathrm{d}|\varepsilon_3|/\mathrm{d}t$). Based on the localised necking time, the localised necking strain was determined using the strains within the local area at the corresponding time. The CC method was applied by analysing the strains within the same local area, as shown in Fig. 9(d). The strain accelerations ($\mathrm{d}^2|\varepsilon_3|/\mathrm{d}t^2$) were calculated by parabolic fit in a fitting window of 7 points in time. Then a correlation coefficient (r_1)

was calculated and the limit strains were determined when r_1 reached the peak of the curve. When using the GCC method, a linear function with slope of 0.05 was added in the strain acceleration, as shown in Fig. 9(e). A gliding correlation coefficient (r_2) was calculated in a window width of 9 points, and the localised necking was determined at the time when r_2 reaches the valley of the curve. Fig. 9(f) shows the application of the GDMM method, in which both the gliding mean ($\bar{x}$) and the gliding median ($\tilde{x}$) of $\mathrm{d}|\varepsilon_3|/\mathrm{d}t$ were calculated in a window width of 7 points. The localised necking strain was determined at the time when $\bar{x} - \tilde{x}$ reaches the peak of the curve.

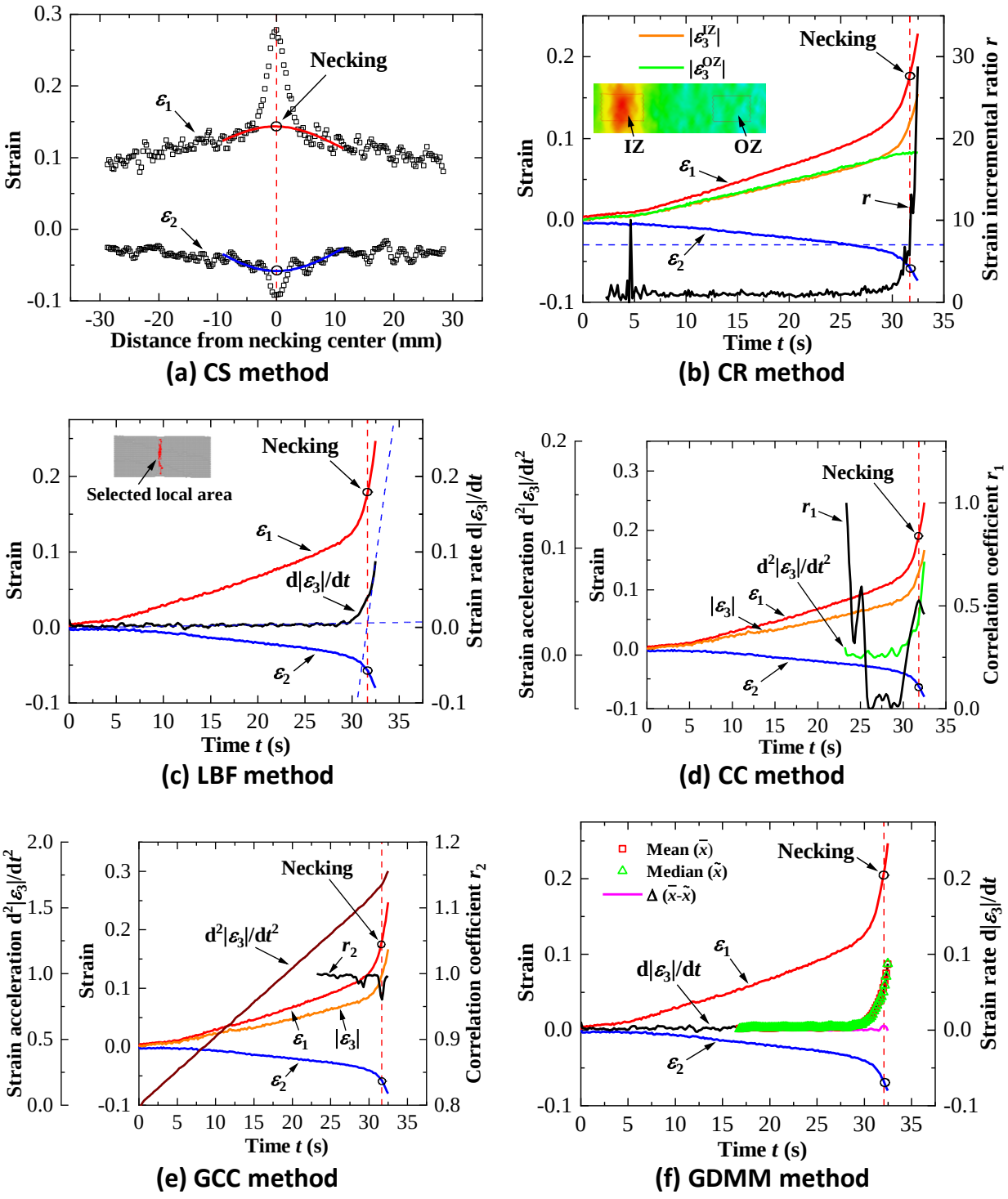

Fig. 9. Determination of localised necking strain for AA7075 sheets, tested in uniaxial tension, using widely employed existing methods: (a) CS method, (b) CR method, (c) LBF method, (d) CC method, (e) GCC method, and (f) GDMM method.

A comparison of localised necking strains for AA7075, determined by the existing methods and the spatio-temporal method, is presented in Fig. 10, using the solid symbols and hollow symbols, respectively. The data corresponding to the CS method were obtained from five predefined cross sections equally spaced in the width direction of the specimen. The data corresponding to the spatio-temporal method were determined by adopting two zone BZ values with W_{BZ} = 2 × h (3.6 mm) and 2.5 × h (4.5 mm) respectively, and with W_L = 3.6 mm and R = 2. The dashed black line is the strain path in the zone BZ with W_{BZ} = W_L = 3.6 mm. It was observed that different localised necking strains were determined by the different methods, and only the major strains ε_{1-LN} determined by the CS method and the spatio-temporal method are in the previously determined range of 0.12 to 0.17. Except for the localised necking strains determined by the CS method where a scatter was observed, values obtained using other methods are on the same strain path and thus the difference between determined localised necking strains can be quantified by comparing ε_{1-LN} only. The GDMM method determined the highest ε_{1-LN} of 0.204 which is 20% higher than the upper bound of 0.17, while the CC method determined a smaller ε_{1-LN} of 0.191, but this is still 12.4% higher than the upper bound. The CR method, the LBF method and the GCC method determined approximatively the same ε_{1-LN} which is 6.5% higher than the upper bound.

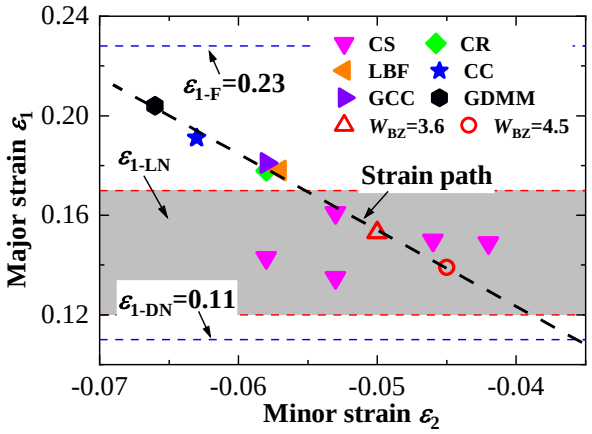

Fig. 10. Comparison of determined localised necking strains of AA7075 sheets, tested in uniaxial tension, using widely employed existing methods and the novel spatio-temporal method with dimensions of zones BZ and RZ as: W_L = 3 mm, R = 2, and W_{BZ} = 2 × h (3.6 mm) and 2.5 × h (4.5 mm) respectively.

The existing methods were also employed to determine localised necking strains for boron steel and AA6082, tested in uniaxial tension and the determined limit strains were compared with that determined using the spatio-temporal method, as shown in Figs. 11(a) and (b) respectively. The data corresponding to the CS method were obtained from five cross sections equally spaced in the width direction of the specimen, and the data corresponding to the spatio-temporal method were determined by adopting two different zone BZ values with W_{BZ} = 2 × h (3 mm) and 2.5 × h (3.75 mm) respectively, and with W_L = 3 mm and R = 2. The dashed black lines represent the strain path in zone BZ with W_{BZ} = W_L = 3 mm. Similar to the observations in the case of AA7075, different localised necking strains were determined by the different methods for both boron steel and AA6082. The major strains ε_{1-LN} determined by the CS method are close to that by the spatio-temporal method. Moreover, the highest ε_{1-LN} was determined by the GDMM method, which is close to or even higher than the ε_{1-F}, as seen in Fig. 11(a) and Fig. 11(b) respectively. The ε_{1-LN} determined by the CC method for boron steel is also close to the ε_{1-F}, while the method was inapplicable to AA6082 due to the scatter of the calculated strain accelerations. In addition, both the LBF method and the GCC method determined major strains ε_{1-LN} which are higher than the upper bound of the previously

determined range. The $\varepsilon_{1-\mathrm{LN}}$ determined by the CR method for boron steel is close to that by the spatio-temporal method, while for AA6082, it is much higher than the latter.

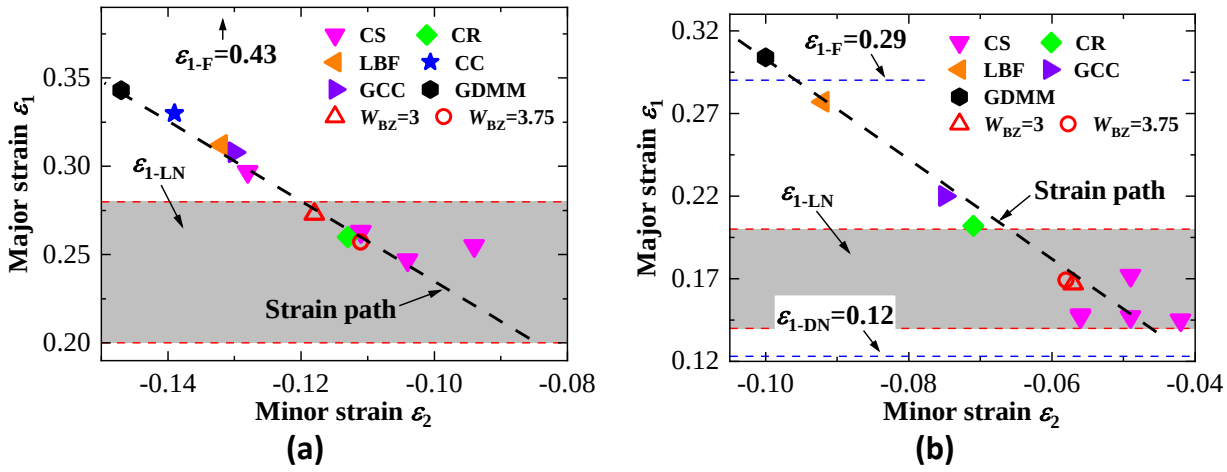

Fig. 11. Comparison of determined localised necking strains of (a) boron steel sheets and (b) AA6082 sheets, tested in uniaxial tension, using widely employed existing methods and the novel spatio-temporal method with dimensions of zones BZ and RZ as: W_{L} = 3 mm, R = 2, and W_{BZ} = 2 × h (3 mm) and 2.5 × h (3.75 mm) respectively.

4.3. Determination of limit strains for AA5754 in biaxial tensile tests

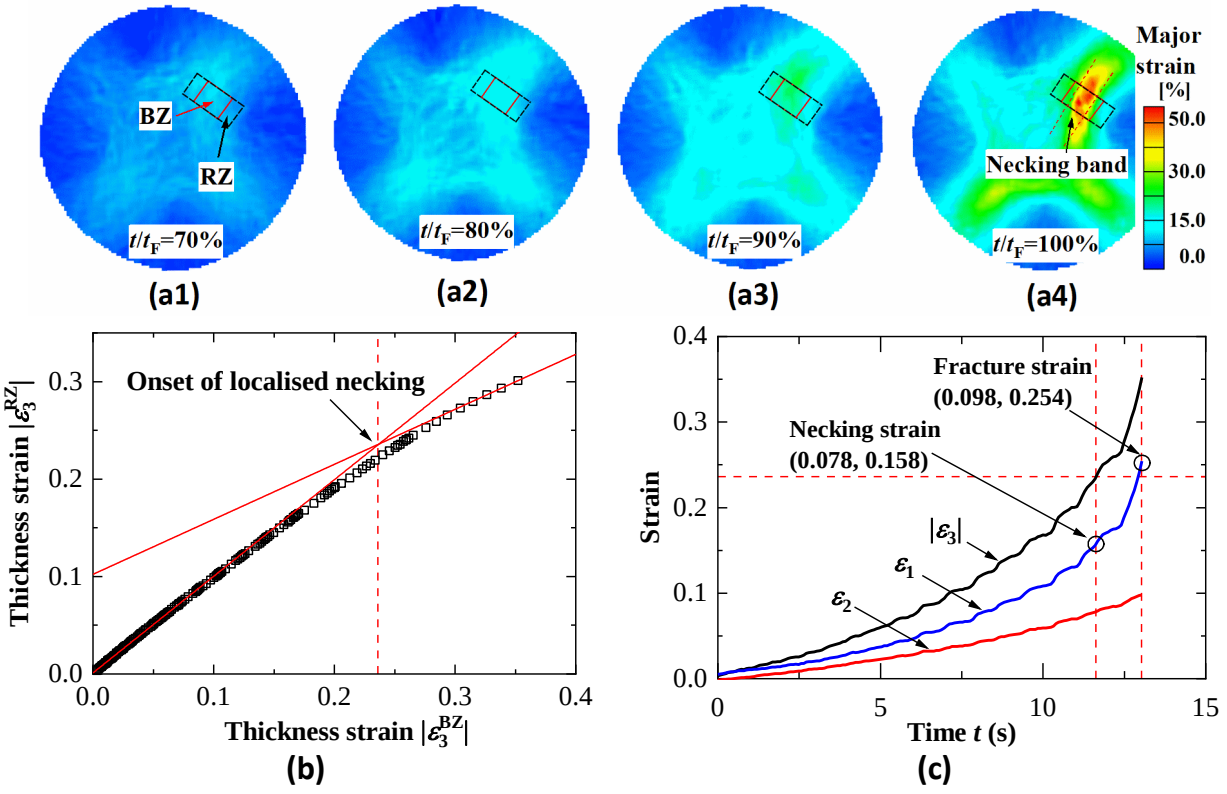

Fig. 12. Application of the novel spatio-temporal method to determine localised necking and fracture strains of AA5754 sheets, subjected to equi-biaxial tension in biaxial tensile tests: (a1)-(a4) major strain contours in the central region of a cruciform specimen at different normalised times (a1) 70%, (a2) 80%, (a3) 90% and (a4) 100%, (b) identification of onset of localised necking with selected zones BZ and RZ, as illustrated in (a1)-(a4), with recommended dimensions W_{BZ} = W_{L} = 1 mm and R = 2, and (c) determination of localised necking and fracture strains.

The novel spatio-temporal method was applied to specimens deformed in the biaxial tensile tests, to determine both localised necking strain and fracture strain for AA5754. Figs. 12(a1)-(a4) show major

strain (engineering) contours, at normalised times t/t_F = 70%, 80%, 90% and 100%, in the central region of a cruciform specimen. A well-developed necking band was observed at t/t_F = 100%, and thus zones BZ and RZ with $W_{BZ} = W_L$ = 1 mm and R = 2 were selected on this image and were transferred on the first image. Fig. 12(b) shows the determination of the onset of localised necking in the space of $|\varepsilon_3^{BZ}|$ versus $|\varepsilon_3^{RZ}|$. As expected, $|\varepsilon_3^{BZ}|$ and $|\varepsilon_3^{RZ}|$ had same values initially, while with increasing the deformation, an increasing difference between the strains appeared. Consequently, both t_{LN} and t_F were determined using the spatio-temporal method and corresponding localised necking strain and fracture strain were determined within the zone BZ, as shown in Fig. 12(c).

For comparison with the proposed method, both the CR method and the LBF method were used to determine the localised necking strain. The dimensions of zones IZ and OZ adopted in the CR method are 1 × 1 mm. Considering the nonuniform strain field outside the necking band, two different zones, OZ-I and OZ-II, were selected for a comparison. The absolute values of average thickness strain within zones IZ ($|\varepsilon_3^{IZ}|$) and OZ ($|\varepsilon_3^{OZ}|$) were plotted in Fig. 13(a), in which serrated plastic flow was observed due to the presence of the PLC effect. In order to reduce the influence of noise, a time interval of 0.8 s was chosen for calculating thickness strain increments. Further, ratios of the increments of strain within zone IZ to that within zones OZ, were calculated, namely $\mathrm{d}|\varepsilon_3^{IZ}|/\mathrm{d}|\varepsilon_3^{OZ-I}|$ and $\mathrm{d}|\varepsilon_3^{IZ}|/\mathrm{d}|\varepsilon_3^{OZ-II}|$, as shown in Fig. 13(a). It is shown that the ratios related to either the OZ-I or the OZ-II strongly fluctuated around a value of one during the whole deformation. This leads to an invalid mathematical evaluation when applying the CR method, due to the PLC effect. Also an attempt was made to use the LBF method to determine localised necking strain. For convenience, $|\varepsilon_3^{IZ}|$ was analysed and a time interval of 0.8 s was chosen for the calculating thickness strain rate ($\mathrm{d}|\varepsilon_3^{IZ}|/\mathrm{d}t$), in order to reduce the influence of noise, as shown in Fig. 13(b). Strong fluctuation was observed in the curve of the thickness strain rate, thereby leading to the failure of the LBF method to determine localised necking strain. This is due to the PLC effect exhibited in AA5754 sheets, which results in serrated strain vs. time curves [33], as shown in Fig. 12(b). Different from the influence of noise from the DIC measurement, fluctuation in calculated strain rate of serrated strain-time data cannot be eliminated by using the smoothing method as suggested in [18]. Given that either strain rate or strain acceleration rate has to be calculated, the other time-dependent methods, such as, CC, GCC, and GDMM, also cannot be used in this case.

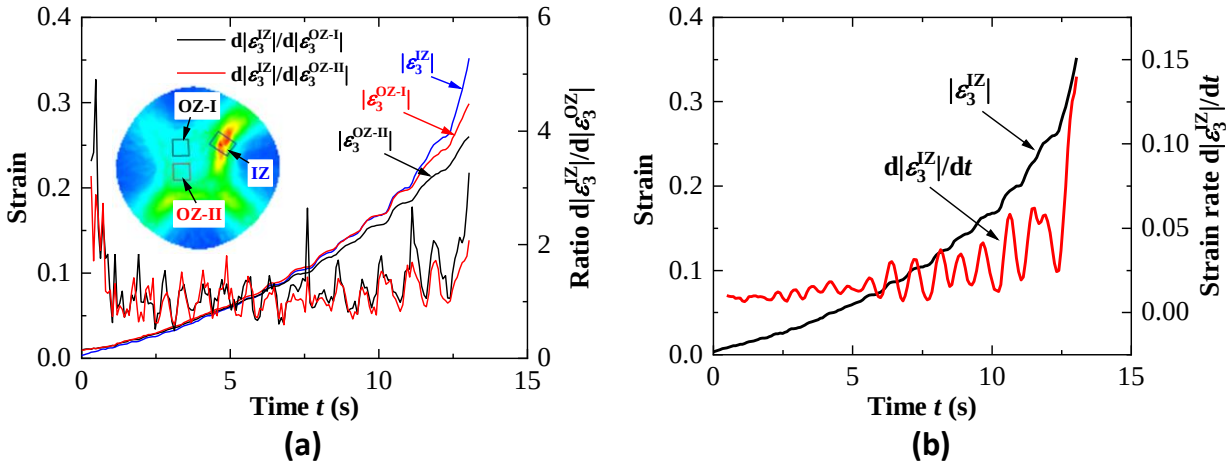

Fig. 13. Challenges when applying the widely used existing methods to determine localised necking strain of AA5754 sheets in biaxial tensile test: (a) incremental ratios of average thickness strain within zone IZ to that within zones OZ-I ($\mathrm{d}|\varepsilon_3^{IZ}|/\mathrm{d}|\varepsilon_3^{OZ-I}|$) and OZ-II ($\mathrm{d}|\varepsilon_3^{IZ}|/\mathrm{d}|\varepsilon_3^{OZ-II}|$), which are necessary for the CR method application, and (b) average

thickness strain rate ($\mathrm{d}|\varepsilon_3^{\mathrm{IZ}}|/\mathrm{d}t$) in the zone IZ, which is necessary for the LBF method application. Both show the fluctuating nature which cannot be used for determination of the localised necking strain.

Localised necking strain for AA5754 subjected to the plane-strain tension in the biaxial tensile test was also determined using the spatio-temporal method. Figs. 14(a1)-(a4) show the major strain contours, at normalised times t/t_{F} = 70%, 80%, 90% and 100%, in the central region of a cruciform specimen. A well-developed necking band was observed in the strain contour at t/t_{F} = 100%, and then zones BZ and RZ with W_{BZ} = W_{L} = 1 mm and R = 2 were selected. Fig. 14(b) shows identification of the onset of localised necking in the space of $|\varepsilon_3^{\mathrm{BZ}}|$ versus $|\varepsilon_3^{\mathrm{RZ}}|$. Similar to the equi-biaxial tension, $|\varepsilon_3^{\mathrm{BZ}}|$ and $|\varepsilon_3^{\mathrm{RZ}}|$ had same values initially, and with increasing of deformation, $|\varepsilon_3^{\mathrm{BZ}}|$ became higher than $|\varepsilon_3^{\mathrm{RZ}}|$ gradually. It is noteworthy that although one straight line was fitted through the last three points immediately before fracture, most points after the appearance of the increasing difference between $|\varepsilon_3^{\mathrm{BZ}}|$ and $|\varepsilon_3^{\mathrm{RZ}}|$ are on the line. Based on the determined t_{LN} and t_{F}, both the localised necking strain and the fracture strain were determined, as shown in Fig. 14(c).

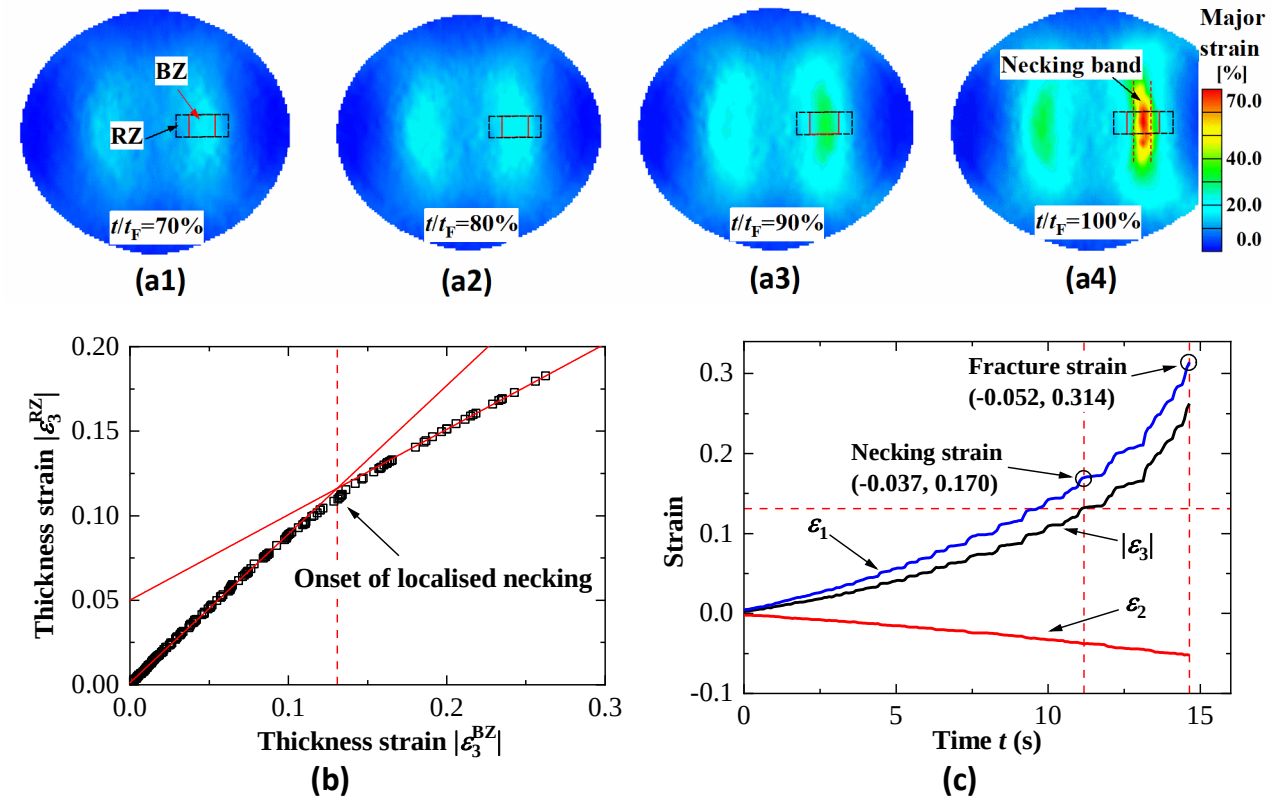

Fig. 14. Application of the novel spatio-temporal method to determine localised necking and fracture strains of AA5754 sheets, subjected to plane-strain tension in biaxial tensile tests: (a1)-(a4) major strain contours in the central region of a cruciform specimen at different normalised times (a1) 70%, (a2) 80%, (a3) 90% and (a4) 100%, (b) identification of onset of localised necking with selected zones BZ and RZ, as illustrated in (a1)-(a4), with the recommended dimensions W_{BZ} = W_{L} = 1 mm and R = 2, and (c) determination of localised necking and fracture strains.

5. Discussion

Using the recommended dimensions given in Table 2, the novel spatio-temporal method can be used to ensure accurate determination of localised necking strain. As seen in Fig. 6(c), Fig. 7(d) and Fig. 8, the localised necking strains, determined using this method, are slightly dependent on the dimensions of zones BZ and RZ, particularly on the dimension orthogonal to the necking band. This is due to inevitable heterogeneous deformation after the onset of necking. By adopting the

recommended dimensions which are related to the thickness of a test-piece, the determined major strains at onset of localised necking were well situated in the reasonable ranges obtained according to the strain distribution around the necking band, as presented in Fig. 4(c), Fig. 7(c) and Fig. 8(c).

Compared with the existing methods, the spatio-temporal method is more simple and stable in determining localised necking strains. It should be noted that the major strains within the two zones can be adopted for identifying onset of localised necking because of the similar distribution and evolution to those of the thickness strains. In the CS method, complicated procedures are usually performed to best fit an inverse parabola in order to determine the localised necking strains [9], which limits its application range. Furthermore, limit strains determined using the CS method are scattered when different cross sections are adopted, as illustrated in Fig. 10 and Fig. 11. Although the CR method is easy to use to determine localised necking strains, noise is a big influence on calculation of strain increment ratios and as a result, the method sometimes becomes inapplicable for the determination, as seen in Fig. 9(b). Other available methods, including, LBF, CC, GCC and GDMM, are based on either strain rate or strain acceleration to identify the onset of localised necking. However, calculations of strain rate and strain acceleration are strongly influenced by noise also.

In addition, the spatio-temporal method is more accurate compared with other existing methods. As seen in Fig. 10 and Fig. 11, localised necking strains determined using the spatio-temporal method are close to that resulting from using the CS method. The determined major strains at onset of localised necking by the CC method and the GDMM method are close to the major strains at fracture, which indicates that the two methods may provide overestimated values. This is consistent with the conclusion in [21]. Although the major strains at onset of localised necking determined by the LBF method and the GCC method are much smaller than the major strains at fracture, they are still higher than the upper bound of the reasonable range. Therefore, the LBF method and the GCC method may also overestimate the localised necking strains. Corresponding to the CR method, the determined major strain at onset of localised is either higher than the upper bound of the range (Fig. 10) or in the middle of the range (Fig. 11(a)), which reveals instability of the CR method in determining the localised necking strains.

One of the great advantages of the spatio-temporal method is the capability of determining the localised necking strain for AA5754 in biaxial tensile tests, which involves noise and the PLC effect. The CS method becomes inapplicable for such tests due to the failure of parabolic fitting [9], in which the fitting width on each side of the crack should be at least 4 mm. The CR method had been used in [24-26] to determine the localised necking strain for AA5086 in a biaxial tensile test. However, different values of 8 [24, 25] and 7 [26] were employed. In addition, as illustrated in Fig. 13(a), calculated strain increment ratios are strongly fluctuated due to influence of the PLC effect, thereby resulting in failure of the method. For the same reason, the time-dependent methods, LBF, CC, GCC and GDMM, also are inapplicable in such tests, as demonstrated in Fig. 13(b).

It is important to note that the spatio-temporal method has the potential to be applied in other formability tests, such as Nakajima tests and Marciniak tests. According to the experimental results presented in [45, 53], strain distributions ranging from uniform deformation to localised necking in specimens deformed in Nakajima tests are similar to that in uniaxial tensile tests. Considering that the onset of localised necking is identified by the beginning of an increasing difference between the thickness strains within two zones, as depicted in Fig. 1, the spatio-temporal method could also be applied in Nakajima tests for limit strain determinations.

6. Conclusions

A novel spatio-temporal method has been proposed to determine localised necking and fracture strains of deformed sheet metals. This could enable us to construct FLDs and FFLDs for sheet metals through various tests, such as biaxial tensile tests. In this method, the onset of localised necking is determined by identifying the beginning of an increasing difference between the thickness strains (or major strains) within two rectangular zones BZ and RZ, with a same central point where localised necking initiates, followed by appearance of a necking band.

Based on the investigations, it is recommended that the dimensions of the two zones BZ and RZ can be chosen according to the following suggestions: (i) in direction parallel to the necking band, the two zones have a same dimension which is in the range of 1.5 to 3 times the sheet thickness; (ii) in orthogonal direction, the dimension of zone BZ is in the range of 2 to 2.5 times the sheet thickness, and the ratio of zone RZ dimension to zone BZ is in the range 2 to 2.5. By adopting the recommended dimensions for the two zones, accurate determinations of limit strains can be realised.

Compared with the other existing methods, the spatio-temporal method is more simple, more stable and enables results with greater accuracy to be produced. Localised necking strains determined by the spatio-temporal method are close in value to those resulting from use of the CS method. However, the localised necking strains determined by the CS method are scattered when different cross sections are used. Time-dependent methods like, LBF, CC, GCC and GDMM, tend to overestimate localised necking strains, and due to difficulties in accurate calculation of either strain rate or strain acceleration, noise or the PLC effect can lead to failure in production of a sound result. Results using the CR method are also greatly influenced by noise or the PLC effect due to problems with calculating strain increment ratio. In contrast, the proposed spatio-temporal method can easily determine the limit strains even under the influences of noise and the PLC effect. Having the advantages described above, the method described in this research has a high potential to become a standard method for the determination of the limit strains for different kinds of sheet metals.

Acknowledgements

The authors would like to thank financial support from EPSRC (Grant no. EP/R001715/1) on “Lightform: Embedding Materials Engineering in Manufacturing with Light Alloys”. R. Zhang also appreciates financial support from the CSC-Imperial Scholarship (Grant no. 201700260069).

Appendix A1

In the proposed method, the zone RZ is defined to include the zone BZ, as shown in Fig. 1(a). For comparison, zone RZ excluding zone BZ was also selected and investigated for all the cases studied in the research. Fig. A1 shows an example of the necking strain determination for AA6082 in the tensile test by selecting a same zone BZ and four different zones RZ, with zones RZ including zone BZ in Fig. A1(a) and zones RZ excluding zone BZ in Fig. A1(b). It can be seen that including the zone BZ into the zone RZ makes the straight line fitting (i.e. determination of onset of necking) more stable and reasonable, while the zone RZ excluding the zone BZ provides unstable results. This might be due to the error from the DIC measurement and the nature of the deformation of materials. Based on the sensitivity studies, it is recommended that the zone BZ is included in the zone RZ.

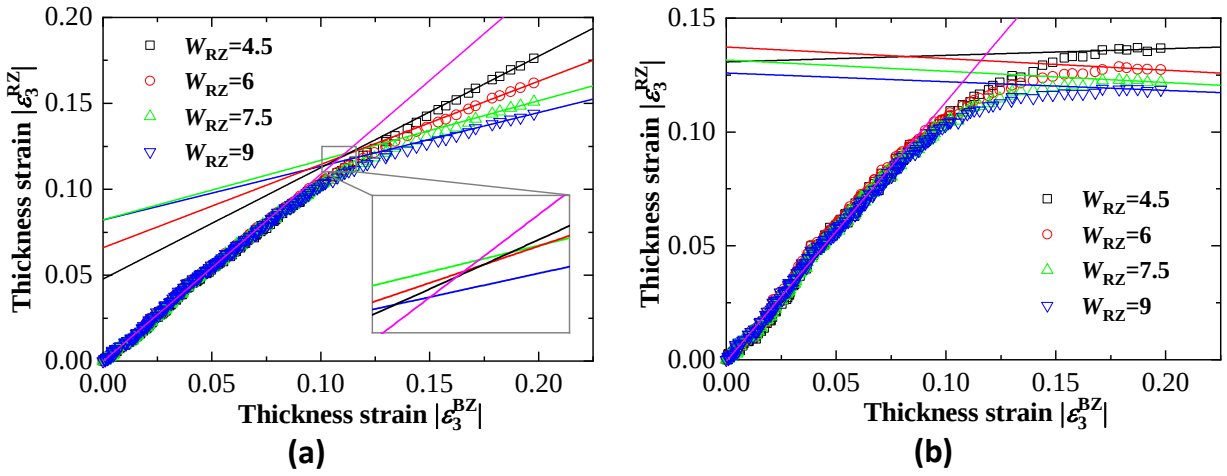

Fig. A1. Necking strain determination in a tensile test for AA6082 by selecting a same zone BZ (W_{BZ} = W_L = 3 mm) and four different zones RZ, (a) zone RZ includes zone BZ, and, (b) zone RZ excludes zone BZ.

Appendix A2

The effect of the dimension W_L on the determined necking strain was investigated by plotting thickness strain within the zones BZ and RZ with different W_L values in the range of $1.5 \times h \leq W_L \leq 3 \times h$, as shown in Fig. A2. It can be seen that in both AA7075 (Fig. A2(a)) and AA6082 (Fig. A2(b)) cases, thickness strain changes little with different W_L values investigated and thus, W_L in the recommended range has little effect on the determined necking strain.

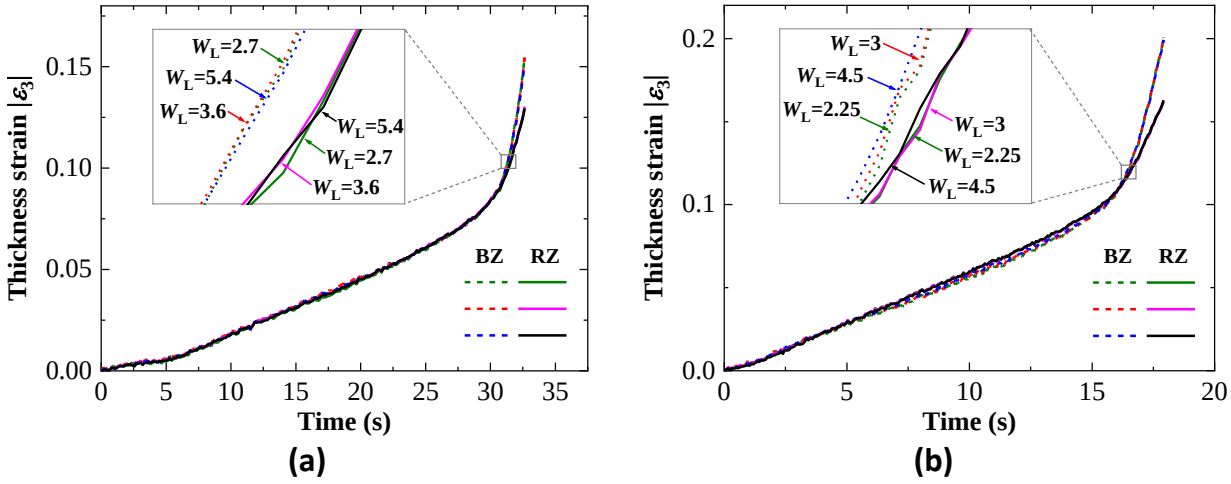

Fig. A2. Absolute values of thickness strain within zones BZ (W_{BZ} = 2 × h) and RZ (W_{RZ} = 2 × W_{BZ}) with different W_L values (1.5 × h, 2 × h and 3 × h) in the uniaxial tensile tests for (a) AA7075 (h = 1.8 mm) and (b) AA6082 (h = 1.5 mm). Both show that W_L has little effect on thickness strain within zones BZ and RZ.

References

[1] S.P. Keeler, Determination of forming limits in automotive stampings, Sheet Metal Industry, 42 (1965) 683-691. doi:10.4271/650535

[2] G.M. Goodwin, Application of strain analysis to sheet metal forming problems in the press shop, SAE Technical Paper, 1968, pp. 380-387. doi:10.4271/680093

[3] J.D. Bressan, J.A. Williams, The use of a shear instability criterion to predict local necking in sheet metal deformation, International Journal of Mechanical Sciences, 25 (1983) 155-168. doi:10.1016/0020-7403(83)90089-9

[4] J. Embury, J. Duncan, Formability maps, Annual Review of Materials Science, 11 (1981) 505-521. doi:10.1146/annurev.ms.11.080181.002445

[5] J. Jeswiet, D. Young, Forming limit diagrams for single-point incremental forming of aluminium sheet, Proceedings of the Institution of Mechanical Engineers, Part B: Journal of Engineering Manufacture, 219 (2005) 359-364. doi:10.1243/095440505x32210

[6] K. Nakazima, T. Kikuma, K. Hasuka, Study on the formability of steel sheets, Yamata Technical Report, (1968) 8517-8530

[7] Z. Marciniak, K. Kuczyński, Limit strains in the processes of stretch-forming sheet metal, International journal of mechanical sciences, 9 (1967) 609-620. doi:10.1016/0020-7403(67)90066-5
[8] J. Min, T. Stoughton, J. Carsley, J. Lin, A method of detecting the onset of localized necking based on surface geometry measurements, Experimental Mechanics, 57 (2017) 521-535. doi:10.1007/s11340-016-0232-4
[9] BS EN ISO 12004, Metallic materials — Sheet and strip — Determination of forming-limit curves Part 2: Determination of forminglimit curves in the laboratory, 2008. doi:10.3403/bseniso12004
[10] J. Min, T.B. Stoughton, J.E. Carsley, J. Lin, An improved curvature method of detecting the onset of localized necking in Marciniak tests and its extension to Nakazima tests, International Journal of Mechanical Sciences, 123 (2017) 238-252. doi:10.1016/j.ijmecsci.2017.02.011
[11] A. Bragard, J.C. Baret, H. Bonnarens, A simplified technique to determine the FLD at onset of necking, Rapport Centre de Recherche de la Metallurgie, (1972) 53-63
[12] E. Affronti, M. Merklein, Analysis of the bending effects and the biaxial pre-straining in sheet metal stretch forming processes for the determination of the forming limits, International Journal of Mechanical Sciences, 138-139 (2018) 295-309. doi:10.1016/j.ijmecsci.2018.02.024
[13] H.J. Bong, F. Barlat, M.-G. Lee, D.C. Ahn, The forming limit diagram of ferritic stainless steel sheets: Experiments and modeling, International Journal of Mechanical Sciences, 64 (2012) 1-10. doi:10.1016/j.ijmecsci.2012.08.009
[14] H. Rong, P. Hu, L. Ying, W. Hou, J. Zhang, Thermal forming limit diagram (TFLD) of AA7075 aluminum alloy based on a modified continuum damage model: Experimental and theoretical investigations, International Journal of Mechanical Sciences, 156 (2019) 59-73. doi:10.1016/j.ijmecsci.2019.03.027
[15] Z. Shi, Y. Wang, J. Lin, T. Dean, D. Balint, M. Stanton, D. Watson, An investigation, using standard experimental techniques, to determine FLCs at elevated temperature for aluminium alloys, The 3rd International Conference on New Forming Technology, Harbin, China, 2012,
[16] L. Zhang, J. Lin, L. Sun, C. Wang, L. Wang, A new method for determination of forming limit diagram based on digital image correlation, SAE Technical Paper, 2013. doi:10.4271/2013-01-1421
[17] K. Wang, J.E. Carsley, B. He, J. Li, L. Zhang, Measuring forming limit strains with digital image correlation analysis, Journal of Materials Processing Technology, 214 (2014) 1120-1130. doi:10.1016/j.jmatprotec.2014.01.001
[18] W. Volk, P. Hora, New algorithm for a robust user-independent evaluation of beginning instability for the experimental FLC determination, International Journal of Material Forming, 4 (2011) 339-346. doi:10.1007/s12289-010-1012-9
[19] G. Huang, S. Sriram, B. Yan, Digital image correlation technique and its application in forming limit curve determination, Proceedings of the IDDRG 2008 International Conference, Olofstrom, Sweden, 2008, pp. 153–162
[20] M. Merklein, A. Kuppert, M. Geiger, Time dependent determination of forming limit diagrams, CIRP Annals - Manufacturing Technology, 59 (2010) 295-298. doi:10.1016/j.cirp.2010.03.001
[21] W. Hotz, M. Merklein, A. Kuppert, H. Friebe, M. Klein, Time dependent FLC determination comparison of different algorithms to detect the onset of unstable necking before fracture, Key Eng Mater, 2013, pp. 397-404. doi:10.4028/www.scientific.net/kem.549.397
[22] D. Banabic, S. Comsa, P. Jurco, G. Cosovici, L. Paraianu, D. Julean, FLD theoretical model using a new anisotropic yield criterion, Journal of Materials Processing Technology, 157 (2004) 23-27. doi:10.1016/j.jmatprotec.2004.09.015
[23] A.B. Da Rocha, F. Barlat, J. Jalinier, Prediction of the forming limit diagrams of anisotropic sheets in linear and non-linear loading, Materials Science and Engineering, 68 (1985) 151-164. doi:0.1016/0025-5416(85)90404-5
[24] I. Zidane, D. Guines, L. Leotoing, E. Ragneau, Development of an in-plane biaxial test for forming limit curve (FLC) characterization of metallic sheets, Measurement Science and Technology, 2010, pp. 055701. doi:10.1088/0957-0233/21/5/055701
[25] L. Leotoing, D. Guines, I. Zidane, E. Ragneau, Cruciform shape benefits for experimental and numerical evaluation of sheet metal formability, Journal of Materials Processing Technology, 213 (2013) 856-863. doi:10.1016/j.jmatprotec.2012.12.013
[26] L. Leotoing, D. Guines, Investigations of the effect of strain path changes on forming limit curves using an in-plane biaxial tensile test, International Journal of Mechanical Sciences, 99 (2015) 21-28. doi:10.1016/j.ijmecsci.2015.05.007
[27] X. Song, L. Leotoing, D. Guines, E. Ragneau, Characterization of forming limits at fracture with an optimized cruciform specimen: Application to DP600 steel sheets, International Journal of Mechanical Sciences, 126 (2017) 35-43. doi:10.1016/j.ijmecsci.2017.03.023
[28] A.J. Martínez-Donaire, F.J. García-Lomas, C. Vallellano, New approaches to detect the onset of localised necking in sheets under through-thickness strain gradients, Materials & Design, 57 (2014) 135-145. doi:10.1016/j.matdes.2014.01.012
[29] R.A. Iquilio, F.M.C. Cerda, A. Monsalve, C.F. Guzmán, S.J. Yanez, J.C. Pina, F. Vercruysse, R.H. Petrov, E.I. Saavedra, Novel experimental method to determine the limit strain by means of thickness variation, International Journal of Mechanical Sciences, 153-154 (2019) 208-218. doi:10.1016/j.ijmecsci.2019.01.036
[30] L. Huang, M. Shi, Determination of the Forming Limit Curve Using Digital Image Correlation-Comparison of Different Approaches to Pinpoint the Onset of Localized Necking, SAE Technical Paper, 2017. doi:10.4271/2017-01-0301
[31] P.D. Zavattieri, V. Savic, L.G. Hector Jr, J.R. Fekete, W. Tong, Y. Xuan, Spatio-temporal characteristics of the Portevin–Le Châtelier effect in austenitic steel with twinning induced plasticity, International Journal of Plasticity, 25 (2009) 2298-2330. doi:10.1016/j.ijplas.2009.02.008
[32] A. Benallal, T. Berstad, T. Børvik, O.S. Hopperstad, I. Koutiri, R.N. de Codes, An experimental and numerical investigation of the behaviour of AA5083 aluminium alloy in presence of the Portevin–Le Chatelier effect, International Journal of Plasticity, 24 (2008) 1916-1945. doi:10.1016/j.ijplas.2008.03.008
[33] X. Song, L. Leotoing, D. Guines, E. Ragneau, Investigation of the forming limit strains at fracture of AA5086 sheets using an in-plane biaxial tensile test, Engineering Fracture Mechanics, 163 (2016) 130-140. doi:10.1016/j.engfracmech.2016.07.007
[34] M. Gorji, B. Berisha, P. Hora, F. Barlat, Modeling of localization and fracture phenomena in strain and stress space for sheet metal forming, International Journal of Material Forming, 9 (2015) 573-584. doi:10.1007/s12289-015-1242-y
[35] S. Panich, M. Liewald, V. Uthaisangsuk, Stress and strain based fracture forming limit curves for advanced high strength steel sheet, International Journal of Material Forming, 11 (2018) 643-661. doi:10.1007/s12289-017-1378-z
[36] N. Park, H. Huh, J.W. Yoon, Anisotropic fracture forming limit diagram considering non-directionality of the equi-biaxial fracture strain, International Journal of Solids and Structures, 151 (2018) 181-194. doi:10.1016/j.ijsolstr.2018.01.009
[37] Y. Lou, H. Huh, S. Lim, K. Pack, New ductile fracture criterion for prediction of fracture forming limit diagrams of sheet metals, International Journal of Solids and Structures, 49 (2012) 3605-3615. doi:10.1016/j.ijsolstr.2012.02.016

[38] Y. Bao, T. Wierzbicki, On fracture locus in the equivalent strain and stress triaxiality space, International Journal of Mechanical Sciences, 46 (2004) 81-98. doi:10.1016/j.ijmecsci.2004.02.006
[39] T. Wierzbicki, Y. Bao, Y.-W. Lee, Y. Bai, Calibration and evaluation of seven fracture models, International Journal of Mechanical Sciences, 47 (2005) 719-743. doi:10.1016/j.ijmecsci.2005.03.003
[40] P.A.F. Martins, L. Kwiatkowski, V. Franzen, A.E. Tekkaya, M. Kleiner, Single point incremental forming of polymers, CIRP Annals, 58 (2009) 229-232. doi:10.1016/j.cirp.2009.03.095
[41] K. Jawale, J.F. Duarte, A. Reis, M.B. Silva, Characterizing fracture forming limit and shear fracture forming limit for sheet metals, Journal of Materials Processing Technology, 255 (2018) 886-897. doi:10.1016/j.jmatprotec.2018.01.035
[42] A. Zahedi, B. Mollaei Dariani, M.J. Mirnia, Experimental determination and numerical prediction of necking and fracture forming limit curves of laminated Al/Cu sheets using a damage plasticity model, International Journal of Mechanical Sciences, 153–154 (2019) 341–358. doi:10.1016/j.ijmecsci.2019.02.002
[43] A.E. Bayoumi, R. Joshi, On the formabllity/instability of stretch-forming sheet metals, Applied Mechanics Reviews, 45 (1992) 154-164. doi:10.1115/1.3121386
[44] R. Hill, On discontinuous plastic states, with special reference to localized necking in thin sheets, Journal of the Mechanics and Physics of Solids, 1 (1952) 19-30. doi:10.1016/0022-5096(52)90003-3
[45] P. Hora, B. Berisha, M. Gorji, N. Manopulo, A generalized approach for the prediction of necking and rupture phenomena in the sheet metal forming, Proceedings of the IDDRG 2012 International Conference, Mumbai, India, 2012, pp. 79-93
[46] Z. Shao, N. Li, J. Lin, T. Dean, Formability evaluation for sheet metals under hot stamping conditions by a novel biaxial testing system and a new materials model, International Journal of Mechanical Sciences, 120 (2017) 149-158. doi:10.1016/j.ijmecsci.2016.11.022
[47] J. Lin, N. Li, Z. Shao, B. Qian, Planar test system, United States 'Patent' US 20180238784 A1, (2018), Aug. 23, 2018.
[48] W. Ma, B. Wang, L. Yang, X. Tang, W. Xiao, J. Zhou, Influence of solution heat treatment on mechanical response and fracture behaviour of aluminium alloy sheets: An experimental study, Materials & Design, 88 (2015) 1119-1126. doi:10.1016/j.matdes.2015.09.044
[49] A. Considère, Mémoire sur l'emploi du fer et de l'acier dans les constructions, Annales des Ponts et Chaussées, 9 (1885) 574-775
[50] Y. Ling, Uniaxial true stress-strain after necking, AMP Journal of technology, 5 (1996) 37-48
[51] A.K. Ghosh, Strain localization in the diffuse neck in sheet metal, Metallurgical Transactions, 5 (1974) 1607-1616. doi:10.1007/bf02646332
[52] M. Zhou, Y. Li, Q. Hu, X. Li, J. Chen, Investigations on edge quality and its effect on tensile property and fracture patterns of QP980, Journal of Manufacturing Processes, 37 (2019) 509-518. doi:10.1016/j.jmapro.2018.12.028
[53] Z. Shao, Q. Bai, N. Li, J. Lin, Z. Shi, M. Stanton, D. Watson, T. Dean, Experimental investigation of forming limit curves and deformation features in warm forming of an aluminium alloy, Proceedings of the Institution of Mechanical Engineers, Part B: Journal of Engineering Manufacture, 232 (2018) 465-474. doi:10.1177/0954405416645776